Activation of Cardiac Progenitor Cells Reverses the Failing Heart Senescent Phenotype and Prolongs Lifespan

Arantxa Gonzalez,* Marcello Rota,* Daria Nurzynska,* Yu Misao, Jochen Tillmanns, Caroline Ojaimi, M. Elena Padin-Iruegas, Patrick Müller, Grazia Esposito, Claudia Bearzi, Serena Vitale, Buddhadeb Dawn, Santosh K. Sanganalmath, Mathue Baker, Thomas H. Hintze, Roberto Bolli, Konrad Urbanek, Toru Hosoda, Piero Anversa, Jan Kajstura, Annarosa Leri

Abstract—Heart failure is the leading cause of death in the elderly, but whether this is the result of a primary aging myopathy dictated by depletion of the cardiac progenitor cell (CPC) pool is unknown. Similarly, whether current lifespan reflects the ineluctable genetic clock or heart failure interferes with the genetically determined fate of the organ and organism is an important question. We have identified that chronological age leads to telomeric shortening in CPCs, which by necessity generate a differentiated progeny that rapidly acquires the senescent phenotype conditioning organ aging. CPC aging is mediated by attenuation of the insulin-like growth factor-1/insulin-like growth factor-1 receptor and hepatocyte growth factor/c-Met systems, which do not counteract any longer the CPC renin–angiotensin system, resulting in cellular senescence, growth arrest, and apoptosis. However, pulse-chase 5-bromodeoxyuridine–labeling assay revealed that the senescent heart contains functionally competent CPCs that have the properties of stem cells. This subset of telomerase-competent CPCs have long telomeres and, following activation, migrate to the regions of damage, where they generate a population of young cardiomyocytes, reversing partly the aging myopathy. The senescent heart phenotype and heart failure are corrected to some extent, leading to prolongation of maximum lifespan. **(*Circ Res*. 2008;102:597-606.)**

Key Words: aging cardiomyopathy ■ cardiac stem cells ■ telomere–telomerase system

Heart failure is the leading cause of death in the elderly, but whether this is the result of a primary aging myopathy or the consequence of coronary artery disease is unknown. In humans, it is difficult to separate the inevitable pathology of the coronary circulation with age from the intrinsic mechanisms of myocardial aging and heart failure. The aging heart typically shows a decreased functional reserve and limited capacity to adapt to cardiac diseases. Although the old heart cannot accommodate sudden increases in pressure and volume loads,[1] the critical question is whether the etiology of ventricular decompensation in the elderly is the product of aging-associated events or the result of primary aging effects on the pool and function of cardiac progenitor cells (CPCs). A related question is whether average lifespan reflects the ineluctable genetic clock[2] or whether heart failure interferes with the programmed death of the organ and organism, negatively affecting lifespan.

With the exception of a few hematological disorders,[3] stem cell failure does not occur in self-renewing organs, including the human heart. Functionally competent CPCs are present in the hearts of patients who die acutely after a large myocardial infarct or undergo cardiac transplantation for end-stage ischemic cardiomyopathy.[4] Similarly, cycling CPCs with long telomeres have been identified in the old decompensated human heart.[5] Functional CPCs may not sense signals from the regions of damage, or their activation, growth, and migration may be impaired, and these variables interfere with the ability of resident CPCs to repair the old heart and preserve its youth. These issues have been addressed in the current study, in which an animal model of normal aging has been used to determine the role that CPCs have in physiological aging and establish whether chronological age impacts on the number and properties of CPCs. Additionally, we tested whether myocardial aging can be reversed by repopulating the senescent heart with new myocytes derived from differentiation of locally activated CPCs. Ultimately, the profound restructuring of the old heart was expected to prolong animal lifespan.

Materials and Methods

Male Fischer rats (Harlan, Indianapolis, Ind) of different ages were characterized physiologically, structurally, and biochemically. Sub-

Original received October 6, 2007; revision received December 8, 2007; accepted January 7, 2008.

From the Departments of Anesthesia and Medicine and Division of Cardiology (A.G., M.R., D.N., Y.M., J.T., M.E.P.-I., P.M., G.E., C.B., S.V., M.B., K.U., T.H., P.A., J.K., A.L.), Brigham and Women's Hospital, Harvard Medical School, Boston, Mass; Department of Physiology (C.O., T.H.H.), New York Medical College, Valhalla, New York 10595; and Institute of Molecular Cardiology (B.D., S.K.S., R.B.), University of Louisville, Ky.

This manuscript was sent to James T. Willerson, Consulting Editor, for review by expert referees, editorial decision, and final disposition.

*These authors contributed equally to this work.

Correspondence to Annarosa Leri, MD, Departments of Anesthesia and Medicine and Division of Cardiology, Brigham and Women's Hospital, Harvard Medical School, Boston, MA. E-mail aleri@zeus.bwh.harvard.edu

sequently, animals were injected intramyocardially with hepatocyte growth factor (HGF) and insulin-like growth factor (IGF)-1 to establish the effects of this intervention on myocardial regeneration, organ aging, and animal lifespan. Experimental protocols are described in the online data supplement, available at http://circres.ahajournals.org.

Results

CPC Aging and Death

To define whether myocardial aging is conditioned by alterations in CPC function, we measured the number of CPCs together with the expression of the aging-associated protein $p16^{INK4a}$[6] in male rats at 4, 12, 20, and 28 months. CPCs are lineage-negative (Lin^{neg}) cells that express the stem cell antigens c-kit, MDR-1, and Sca-1, alone or in combination.[7] Lin^{neg} CPCs are clustered in cardiac niches,[8] which are located predominantly in the atria and apex. This study is mostly restricted to c-kit–positive CPCs because of their superior growth and differentiation behavior.[9]

From 4 to 28 months, CPCs increased ≈2.9-fold and $p16^{INK4a}$-positive CPCs ≈12-fold. Similarly, apoptosis increased with age and was restricted to $p16^{INK4a}$-positive CPCs. As a result, the number of functionally competent CPCs remained constant up to 20 months and decreased sharply at 28 months (Figure I in the online data supplement).

CPC Activation and Differentiation

The aging myopathy is characterized by an increased myocyte mitotic index[5] that reflects CPC activation and lineage commitment.[10] Myocyte progenitors/precursors correspond to differentiating CPCs that express c-kit and transcription factors and cytoplasmic proteins specific to myocytes. This documents the linear relationship between CPCs and forming myocytes. CPCs positive for the myocyte transcription factor MEF2C, ie, myocyte progenitors, or both MEF2C and the sarcomeric protein cardiac myosin heavy chain (MHC), ie, myocyte precursors, increased with age (supplemental Figure I).

Pulse-chase 5-bromodeoxyuridine (BrdUrd)-labeling assay was performed[8] because this protocol, together with the identification of c-kit, allowed us to assess whether the senescent heart contained functionally competent CPCs with the properties of stem cells.[11] Rats at 4 and 27 months were exposed to BrdUrd for 7 days, and BrdUrd-positive CPCs were measured at 7 days and after 12 weeks of chasing. Bright and dim BrdUrd-labeled CPCs were discerned by fluorescence intensity to score long-term label-retaining CPCs; this provides a functional identification of resident stem cells.[11]

Recently, the long-term BrdUrd-retaining assay was challenged. The argument was made that isolation of hematopoietic stem cells (HSCs) by fluorescence-activated cell sorting is superior in specificity and sensitivity to the analysis of stem cells at the single-cell level within tissues.[12] Unfortunately, the intensity of BrdUrd fluorescence after chasing was not evaluated. Instead, the number of cells with "detectable" BrdUrd levels was measured. Arbitrarily, the threshold of BrdUrd labeling was set at 6% of the signal of BrdUrd-positive cells at the end of the pulse period; the protocol was arranged to identify BrdUrd-positive cells not to distinguish the distribution of BrdUrd levels in HSCs. It is unrealistic that all examined HSCs experienced the same number of divisions and had identical levels of BrdUrd incorporation. By design, preservation of the BrdUrd signal or its dilution with time was not determined, defeating the purpose of the BrdUrd-retaining assay.

In the current study, after 12 weeks of chasing, the number of BrdUrd-bright CPCs detected at 7 days decreased 86% and 93% in young and old animals, respectively. At 7 days, 532 and 2012 BrdUrd-bright CPCs were found in young and old hearts, respectively. Corresponding values at 12 weeks were 73 and 140; they constituted slow-cycling stem cells (Figure 1A and 1B). From 7 days to 12 weeks, BrdUrd-dim CPCs increased 10-fold in young and 32-fold in old hearts. The number of BrdUrd-bright and BrdUrd-dim CPCs did not change in 12 weeks in young but increased in old animals. Thus, the growth kinetics of CPCs preserves the pool of primitive cells in the young heart but expands this compartment in the old myocardium. The number of BrdUrd-bright CPCs in other self-renewing organs, including the skin and ocular bulb, is several orders of magnitude higher than in the heart.[13,14] However, the heart and bone marrow[15] have similar values.

BrdUrd-positive myocytes were measured at 7 days (supplemental Figure IIA) and 12 weeks. BrdUrd-bright myocytes at 12 weeks were cells that experienced a limited number of divisions, whereas BrdUrd-dim myocytes were considered the progeny of CPCs, which became BrdUrd-positive at the time of exposure and formed a large number of committed cells. Cells with intermediate BrdUrd levels were assumed to represent amplifying myocytes that incorporated BrdUrd at the time of exposure and continued to divide and differentiate. Scattered BrdUrd-positive myocytes were observed at 7 days. Following chasing, clusters of BrdUrd-dim myocytes together with BrdUrd-bright myocytes were detected predominantly in old animals. The percentage of BrdUrd-positive myocytes was 5.3-fold higher in old than in young hearts (Figure 1C and 1D). In both cases, the number of BrdUrd-bright myocytes decreased markedly with chasing, whereas BrdUrd-dim myocytes increased.

The high level of myocyte formation in old hearts was confirmed by the myocyte mitotic index measured in situ and in isolated cells (Figure 1E and 1F and supplemental Figure II). It is remarkable that ≈45% of myocytes were replaced in 12 weeks in senescent animals; this value was ≈5-fold larger than in young rats. However, in spite of this dramatic increase in new myocytes, cell death exceeds myocyte regeneration and the aging myopathy cannot be prevented.[5,16] Additionally, the increased number of cycling cells in the senescent heart is consistent with the enhanced toxicity of anticancer drugs in the elderly.[17]

CPC and Myocyte Senescence

The accumulation of $p16^{INK4a}$-positive myocytes with age[16] may be mediated by differentiation of CPCs with short telomeres, which form a myocyte progeny that rapidly reaches cellular senescence. Therefore, telomere length was measured in c-kit–positive cells (Figure 2A through 2C) and developing myocytes expressing the cell cycle protein Ki67 (supplemental Figure III). Telomere length in CPCs, myocyte progenitors/precursors and developing myocytes was 30%, 35%, and 51% shorter in old than young cells, respectively (Figure 2D); ≈50% of old and ≈15% of young CPCs had telomeres less than 12 kbp and were

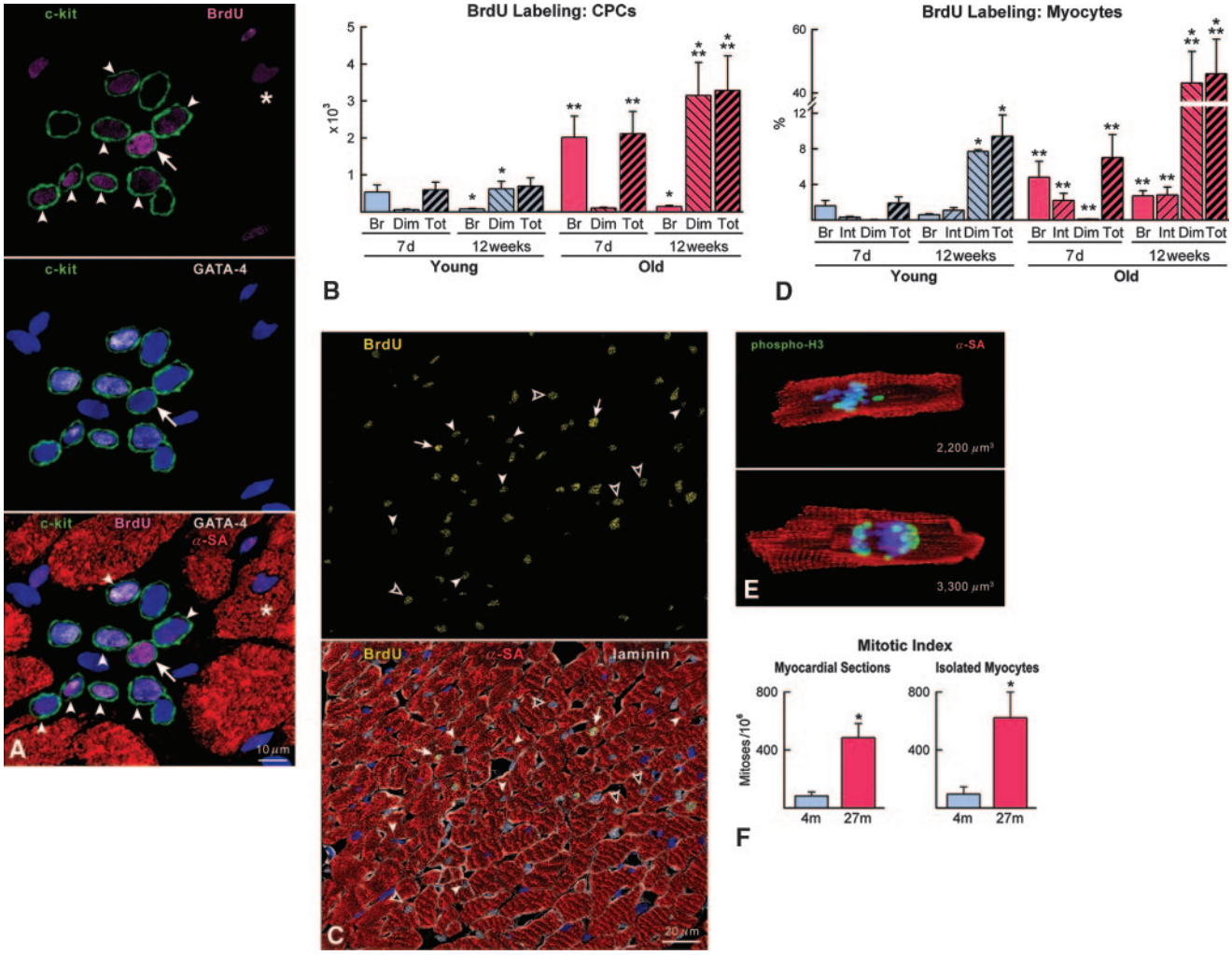

Figure 1. CPC aging and growth. A, Old heart after 12 weeks of chasing: atrial niche in which 1 CPC is BrdUrd-bright (magenta; arrow) and 7 are BrdUrd-dim (arrowheads). The BrdUrd-bright CPCs is Lin^{neg} (GATA-4-negative). One BrdUrd-dim myocyte is visible (α-sarcomeric actin, α-SA, asterisk). B, BrdUrd-bright and -dim CPCs at 7 days and 12 weeks. C, Old LV: BrdUrd (yellow) -bright (arrows), -intermediate (open arrowheads), and -dim (arrowheads) myocytes at 12 weeks. D, BrdUrd-bright, -intermediate, and -dim myocytes at 7 days and 12 weeks. *$P<0.05$ vs 7 days (7d); **$P<0.05$ vs young hearts. E, Metaphase and anaphase chromosomes in dividing myocytes from young (top) and old (bottom) hearts. Phospho-H3, green. F, Myocyte mitotic index. *$P<0.05$ vs young hearts.

$p16^{INK4a}$-positive. However, ≈20% of old CPCs had telomeres >18 kbp, pointing to a relevant growth reserve of the senescent myocardium. Thus, telomere attrition in CPCs with age leads to the generation of a myocyte progeny that acquires quickly the senescent phenotype conditioning organ aging.

CPC Aging and Growth Factor Receptor Systems

The IGF-1/IGF-1R pathway preserves telomere length and promotes CPC growth and survival,[16] whereas CPC migration and homing are predominantly modulated by the HGF/c-Met receptor system.[9] Although the consequences of angiotensin (Ang) II on CPCs are unknown, this growth factor decreases the number and function of endothelial progenitor cells, triggers apoptosis, and is implicated in the progression of heart failure.[18] Therefore, we determined whether aging alters IGF-1/IGF-1R and HGF/c-Met in CPCs and whether CPCs possess a local renin–angiotensin system (RAS), which is influenced by age.

CPCs express IGF-1R, c-Met, and Ang II type 1 (AT_1) receptors, together with IGF-1, HGF, and Ang II (supplemental Figure IV). Detection of Ang II, IGF-1, and HGF in freshly isolated CPCs and tissue sections cannot discriminate whether growth factors are formed within cells or sequestered from the circulation. However, transcripts for renin, angiotensinogen (Aogen), and AT_1 receptor were detected by real-time RT-PCR in CPCs isolated from hearts at 3, 12, 16, and 24 months (Figure 3A and supplemental Figure V). CPC aging resulted in downregulation of Aogen and AT_1 receptors, whereas renin mRNA increased at 12 and 16 months, returning to baseline at 24 months. Although changes in mRNAs occurred with age, the protein levels of Aogen and AT_1 receptors did not vary (Figure 3B), suggesting that RAS function remained intact in old CPCs.

The CPC IGF-1/IGF-1R system was characterized by a significant decrease in IGF-1R mRNA with aging, whereas IGF-1 expression was variable and tended to be reduced only at 24 months. c-Met transcripts were modestly affected in aging CPCs, but HGF mRNA was attenuated at 24 months (Figure 3C and supplemental Figure V).

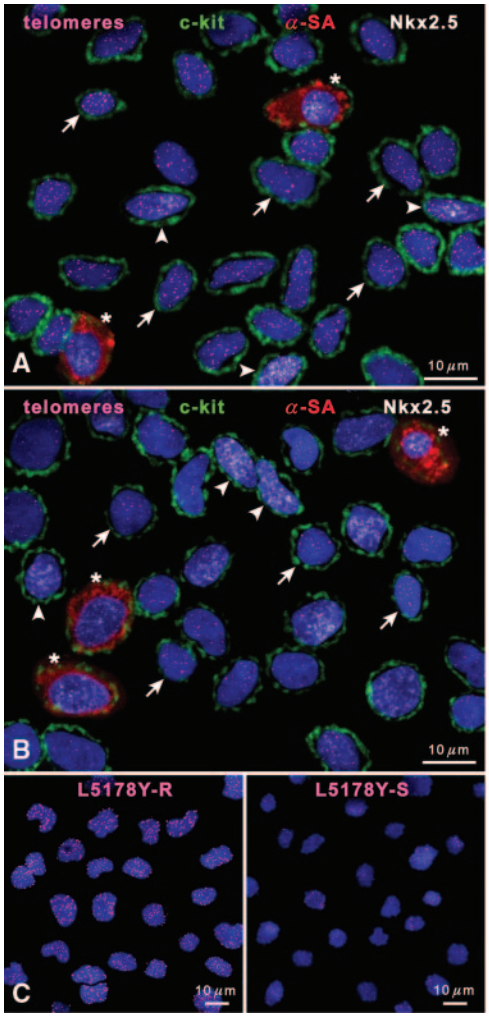

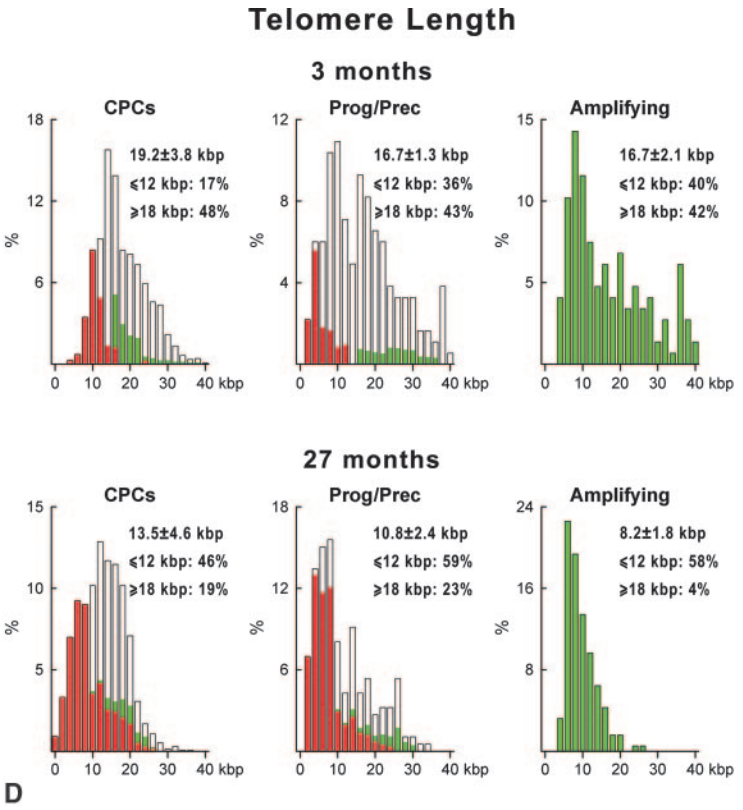

Figure 2. CPCs and telomere length. Telomeres (magenta) in isolated CPCs from young (A) and old (B) hearts. Lin^{neg} CPCs (c-kit, green; arrows), myocyte progenitors (Nkx2.5, white; arrowheads) and myocyte precursors (α-SA, red; asterisks) are present. C, Lymphoma cells with long (L5178Y-R, 48 kbp) and short (L5178Y-S, 7 kbp) telomeres. D, Telomeric length in Lin^{neg} CPCs, myocyte progenitors/precursors and amplifying myocytes in young (top graphs) and old (bottom graphs) hearts. Average telomere length is listed together with the percentage of cells with telomeres ≤12 kbp and ≥18 kbp. Fractions of cycling cells (green solid bars) and senescent p16^{INK4a}-positive cells (red solid bars) are shown.

The ability of CPCs to synthesize IGF-1, HGF, and Ang II was measured. Baseline values for IGF-1 were similar in young and old CPCs, but HGF tended to be lower in old cells. Ang II levels, however, were 3-fold higher in old than in young CPCs (Figure 3D). Following ligand stimulation, IGF-1 formation was 8-fold higher in cells at 3 than at 27 months, whereas HGF synthesis increased 4-fold in young and 3.5-fold in old CPCs. Ang II stimulation did not increase octapeptide synthesis in either cell population. Thus, aging negatively affects regulatory systems involved in CPC growth, survival, and migration, potentiating the detrimental consequences of the local RAS.

CPC Division and Apoptosis

CPCs were cultured in serum-free medium and stimulated with Ang II, IGF-1, HGF, or IGF-1 and HGF together (IGF-1/HGF). The ability of IGF-1, HGF, and IGF-1/HGF to induce CPC proliferation was attenuated but not abolished in old CPCs. Ang II had no growth-promoting effects on CPCs (Figure 4A). Ang II stimulated CPC apoptosis, and IGF-1 decreased the extent of Ang II–mediated CPC death. Conversely, HGF did not decrease apoptosis or enhanced the effects of IGF-1 on CPC survival. Although the inhibitory role of IGF-1 in CPC apoptosis was higher in young than in old cells, a 40% reduction in apoptosis was measured in old CPCs.

A question concerned the impact of Ang II on young and old CPCs because the rate of apoptosis triggered by Ang II was comparable in the 2 cell populations. Ang II leads to the generation of hydroxyl radical, which promotes deoxyguanosine (dG) oxidation, a process that may vary in young and old CPCs. In the presence of hydroxyl radical, the formation of 8-OH-dG lesions is 5-fold higher in telomeric than in nontelomeric DNA.[19] Importantly, 8-OH-dG was detected in a larger fraction of old than young CPCs (Figure 4B through 4D) and Ang II further enhanced this phenomenon, providing a mechanism for Ang II–mediated DNA damage with age.

Aging, CPC Heterogeneity, and Growth

We then established whether these growth factor receptor systems were uniformly affected in aging CPCs or aging progressively involved a larger number of CPCs leaving intact a subset of progenitor cells. The fraction of CPCs positive for IGF-1, IGF-1R, HGF, and c-Met decreased from 3 to 28 months, and the percentage of CPCs expressing Ang II and AT_1 receptors increased (Figure 5A). CPCs expressing IGF-1/IGF-1R and HGF/c-Met were consistently negative for p16^{INK4a}, whereas p16^{INK4a} was detected in CPCs positive for Ang II and AT_1 receptors.

To test whether a small proportion of old CPCs possessed a growth potential similar to young CPCs, CPCs at 3 and 27

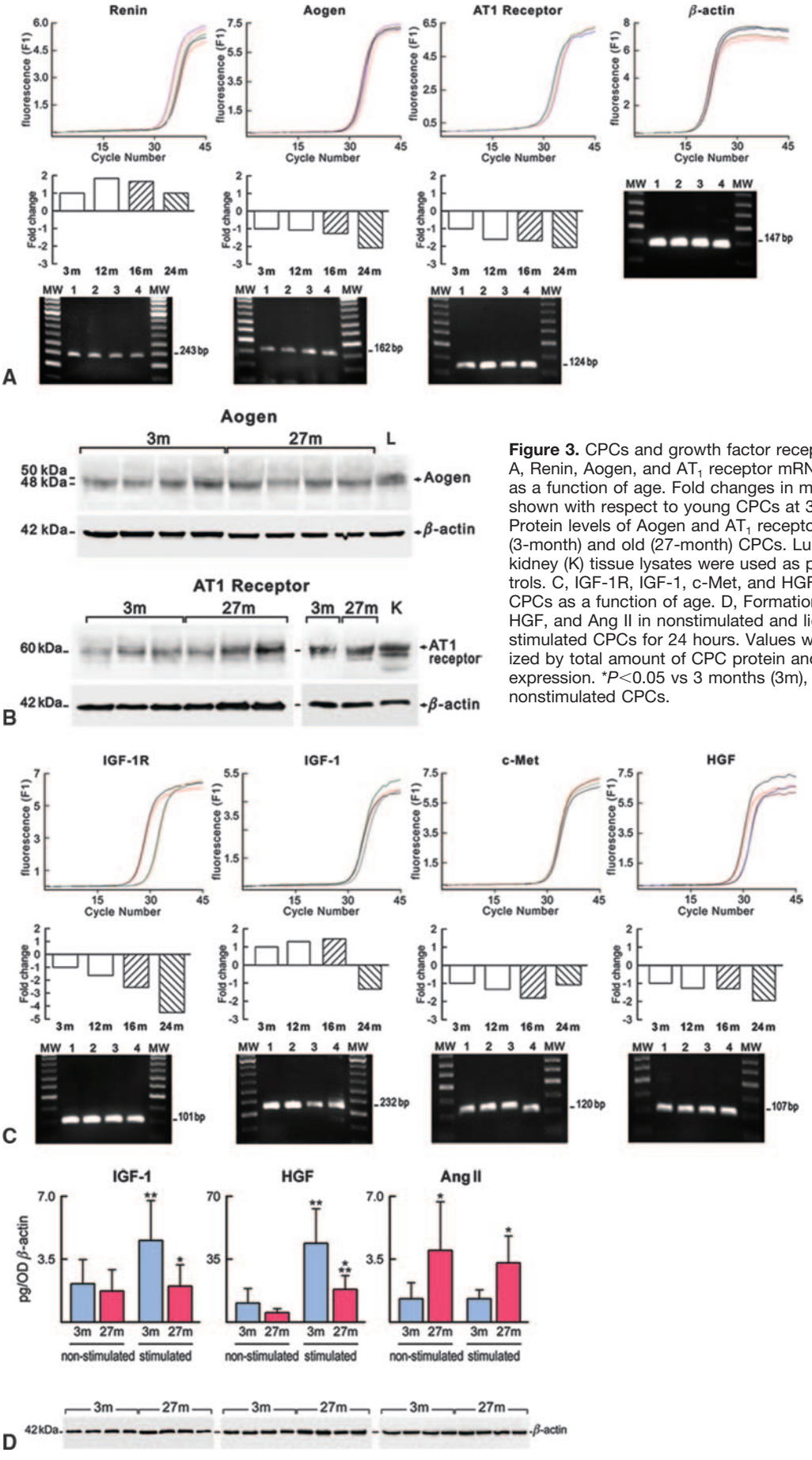

Figure 3. CPCs and growth factor receptor systems. A, Renin, Aogen, and AT_1 receptor mRNAs in CPCs as a function of age. Fold changes in mRNAs are shown with respect to young CPCs at 3 months. B, Protein levels of Aogen and AT_1 receptors in young (3-month) and old (27-month) CPCs. Lung (L) and kidney (K) tissue lysates were used as positive controls. C, IGF-1R, IGF-1, c-Met, and HGF mRNAs in CPCs as a function of age. D, Formation of IGF-1, HGF, and Ang II in nonstimulated and ligand-stimulated CPCs for 24 hours. Values were normalized by total amount of CPC protein and β-actin expression. $^{*}P<0.05$ vs 3 months (3m), $^{**}P<0.05$ vs nonstimulated CPCs.

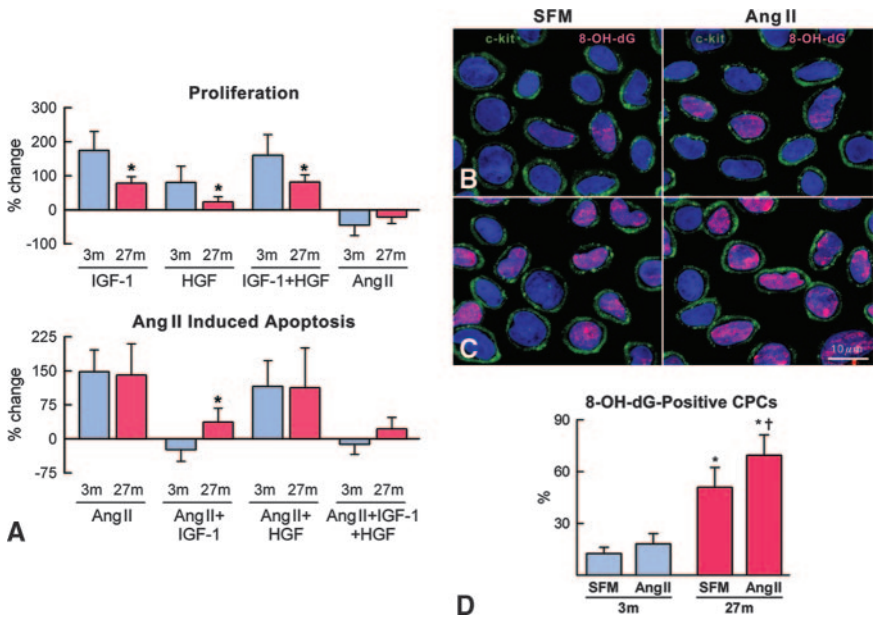

Figure 4. CPCs and IGF-I, HGF, and Ang II. A, Proliferation and apoptosis of young and old CPCs. Percentage changes were computed with respect to nonstimulated CPCs. *$P<0.05$ vs 3 months (3m). Localization of 8-OH-dG (magenta) in young (B) and old (C) CPCs at baseline (left images) and following Ang II stimulation (right images). D, CPCs positive for 8-OH-dG. *$P<0.05$ vs 3 months; †$P<0.05$ vs serum-free medium.

months were serially passaged to reach 20 population doublings. Although the lag-growth phase was longer in old CPCs, the exponential-growth phase was similar in both cell classes (Figure 5B). Similarly, BrdUrd labeling at passage P7 to P8 resulted in comparable levels of BrdUrd-positive CPCs, and telomerase activity in old CPCs decreased only 33% (Figure 5C). Thus, myocardial aging does not deplete the pool of functionally competent CPCs.

CPC Aging and Cell Mobilization

The presence of a compartment of nonsenescent CPCs in the aged heart raised the possibility that these cells may be activated and induced to translocate from their sites of storage in the atria and apex to the base/midregion of the left ventricle (LV). A retroviral vector encoding enhanced green fluorescent protein (EGFP) was injected into the atrioventricular groove to label replicating cells in animals at 4 and 27 months (supplemental Figure VI). A retrovirus was used to infect only replicating cells and avoid cell cycle activation in terminally differentiated myocytes. In both cases, ≈9% to 12% c-kit–positive CPCs were infected with EGFP; this value was consistent with the fraction of Ki67-positive CPCs in this region (data not shown). Two days later, 3 increasing concentrations of HGF were administered

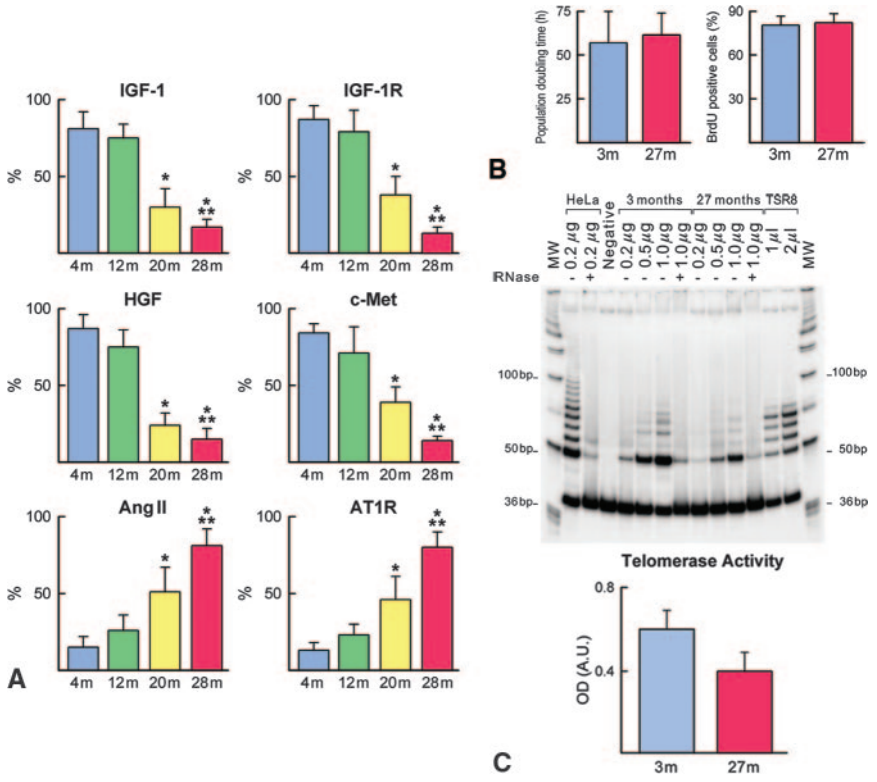

Figure 5. CPC characteristics. A, CPCs positive for IGF-1, IGF-1R, HGF, c-Met, Ang II, and AT_1 receptors. *$P<0.05$ vs 4 months and 12 months, **$P<0.05$ vs 20 months. B, Population doubling time and BrdUrd labeling of CPCs from young (3-month) and old (27-month) hearts. C, Telomerase activity in young (3-month) and old (27-month) CPCs. Telomerase activity starts at 50 bp and displays 6 bp periodicity. HeLa cells were used as positive control, and samples treated with RNase were used as negative control. TSR8 was used to confirm the position of the bands. Three protein concentrations were used to validate the specificity of the assay. The band at 36 bp is an internal control for PCR efficiency.

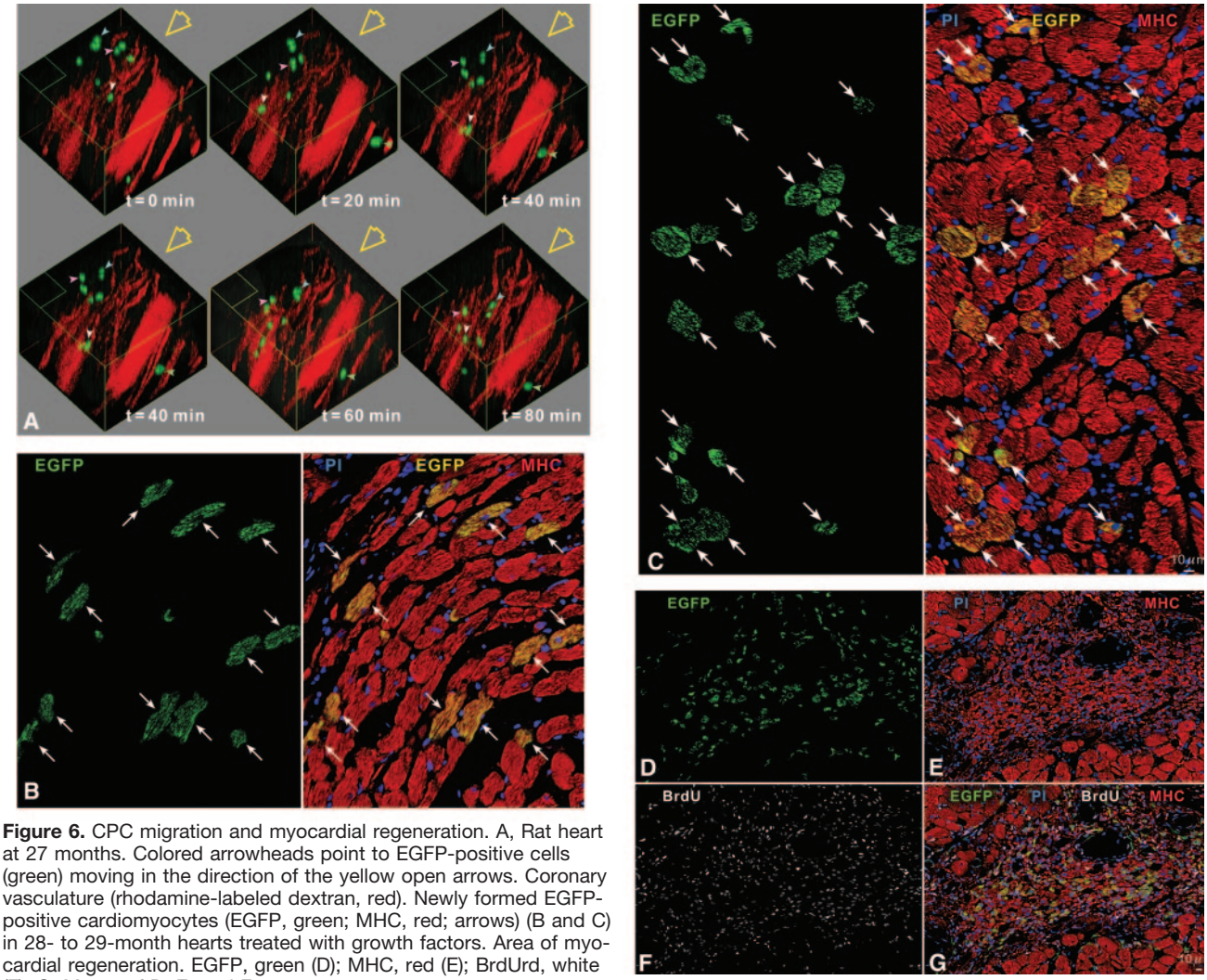

Figure 6. CPC migration and myocardial regeneration. A, Rat heart at 27 months. Colored arrowheads point to EGFP-positive cells (green) moving in the direction of the yellow open arrows. Coronary vasculature (rhodamine-labeled dextran, red). Newly formed EGFP-positive cardiomyocytes (EGFP, green; MHC, red; arrows) (B and C) in 28- to 29-month hearts treated with growth factors. Area of myocardial regeneration. EGFP, green (D); MHC, red (E); BrdUrd, white (F). G, Merge of D, E, and F.

from the site of CPC accumulation in proximity of the atrioventricular groove to the LV midregion (supplemental Figure VI). The migration of EGFP-positive cells was then determined by 2-photon microscopy (supplemental Figures VII through X).

The myocardial area examined by 2-photon microscopy was analyzed subsequently by confocal microscopy to characterize the identity of the migrated EGFP-positive cells. Translocated EGFP-positive cells expressed c-kit, MDR1, or Sca-1 together with c-Met. Moreover, GATA-4 was detected in some cells, documenting their commitment to the myocyte lineage. Ki67 was present in a subset of EGFP-positive cells (supplemental Figures VIII and X).

To determine whether translocation of EGFP-positive cells occurred through the coronary circulation, myocardial interstitium, or both, the coronary vasculature was perfused with rhodamine-labeled dextran, and HGF was injected at the time of observation. Over 5 to 6 hours, none of the moving EGFP-positive cells was found within the lumen of coronary vessels (Figure 6A and supplemental Figure XI); CPCs migrated through the interstitium within tunnels defined by fibronectin.

HGF mobilized and translocated CPCs from the atrioventricular groove toward the LV midregion. Two aging effects were observed: the speed of migration and the number of migrating CPCs were significantly higher in young than in old hearts (supplemental Figure XII). Because of the growth-promoting effects of IGF-1 on CPCs,[9] IGF-1 was injected alone or in combination with HGF, and the number and rate of migration of EGFP-positive cells was determined together with the fraction of cycling EGFP-positive cells. In young and old hearts, IGF-1 failed to stimulate the locomotion of CPCs and to increase the migratory ability of HGF. However, IGF-1 significantly increased the number of dividing CPCs in both young and old hearts (supplemental Figure XII).

Migrating CPCs and their early committed progeny had long telomeres and were $p16^{INK4a}$-negative. This was in contrast to the properties of nontranslocated CPCs in the LV midregion of control hearts. These cells had short telomeres and frequently expressed $p16^{INK4a}$ (supplemental Figure XII). These results suggest that functionally competent CPCs were stored in atrial niches, whereas aging effects were more prominent in the midregion of the LV myocardium.

CPC Aging and Myocardial Regeneration

To test whether the negative effects of aging on the heart could be reversed by activation of resident CPCs, HGF and

IGF-1 were injected intramyocardially into rats at 15, 20, and 27 months of age (supplemental Figure XIII). The animals were euthanized 45 days later. Two days before growth factor administration, the atrioventricular groove and the apex were injected with the EGFP–retrovirus to label cycling CPCs.

In all treated rats, EGFP-positive myocytes, coronary arterioles, and capillaries were identified in the LV midregion (Figure 6B and 6C and supplemental Figure XIV). Conversely, EGFP-positive myocytes and vessels were absent in untreated animals. Frequently, clusters of regenerated myocytes replaced foci of myocardial damage (Figure 6D through 6G). Quantitatively, the number of EGFP-positive myocytes was significantly higher in rats at 28 to 29 months than at 16 to 17 and 21 to 22 months. A similar response was observed for coronary vessels (supplemental Figure XIV).

EGFP-labeled structures reflected only partly the extent of tissue regeneration because ≈9% to 12% CPCs were infected by the EGFP–retrovirus. Thus, BrdUrd was given after the delivery of growth factors or vehicle and was continued throughout to assess cumulative myocyte and vessel formation. Without treatment, myocyte and vessel growth increased with age, pointing to the ability of the old heart to react to tissue injury. Growth factor administration increased cardiomyocyte formation by 55%, 66%, and 88% at 16 to 17, 21 to 22, and 28 to 29 months, respectively (Figure 7A). Vessel regeneration also occurred (supplemental Figure XV). In treated hearts at 28 to 29 months, new myocytes decreased by 20% the number of $p16^{INK4a}$-positive cells (Figure 7B), and this change reflected the increase in BrdUrd-labeled cells.

Remodeling of the Aging Heart and Mortality

Myocardial regeneration mediated by CPC activation attenuated ventricular dilation and the decrease in ventricular mass-to-chamber volume ratio (supplemental Figure XVI), resulting in improvement of cardiac function in animals at 28 to 29 months. Without treatment, heart failure at 27 months deteriorated further at 28 to 29 months. Following treatment, the alterations in ventricular pressures, dP/dt, and diastolic stress at 27 months were no longer apparent at 28 to 29 months (Figure 7C). The anatomy and function of treated hearts at 28 to 29 months became similar to the anatomy and function of untreated hearts at 16 to 17 months (Figure 8A).

Echocardiography was performed in rats at 27 months, 1 day before treatment, and 45 days later, before euthanasia, at 28 to 29 months. Therapy significantly decreased end-diastolic and end-systolic LV diameters, whereas ejection fraction increased 12 percentage points, from 67±7% to 79±7%. The improvement in cardiac function was apparent when early and late echocardiograms were compared (supplemental Figure XVII and Movies I and II). In untreated rats, ventricular hemodynamics deteriorated with time (Figure 8B).

A mortality study was conducted in a cohort of 32 untreated and 48 treated rats at 27 months. By 31 months, all untreated rats were dead. However, 28% of treated rats were alive at 31 months and the last animal died at 33 months (Figure 8C). Growth factor treatment increased life expectancy at 27 months by 44%, from 57 to 82 days.

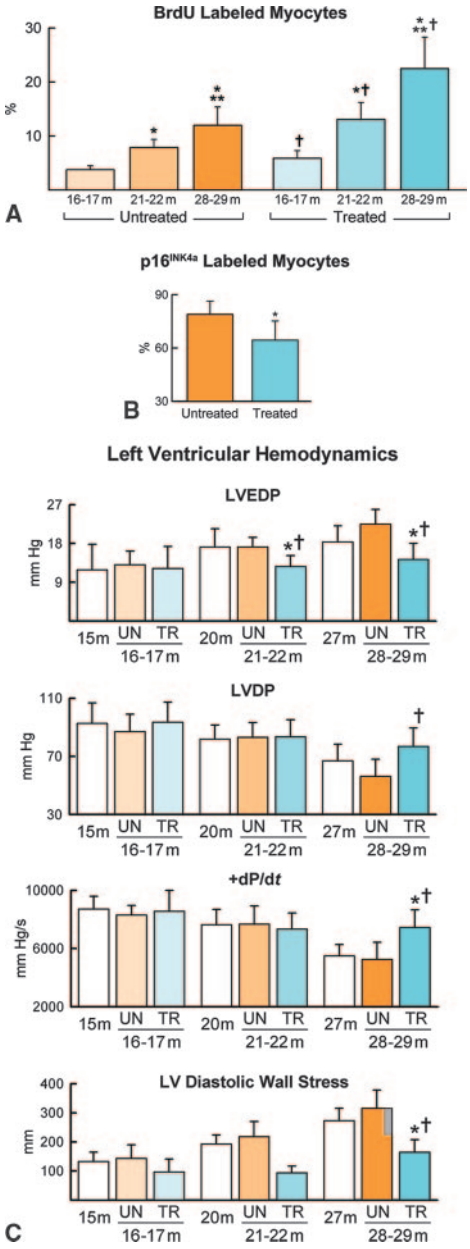

Figure 7. Cardiac anatomy and function. A, BrdUrd-positive myocytes. *$P<0.05$ vs 16 to 17 months, **$P<0.05$ vs 21 to 22 months, †$P<0.05$ vs untreated animals. B, $p16^{INK4a}$-positive myocytes. *$P<0.05$ vs untreated hearts at 28 to 29 months. C, LV hemodynamics at baseline (white bars) and 45 days later in untreated (orange bars) and treated (blue bars) rats. *$P<0.05$ vs baseline, †$P<0.05$ vs untreated animals.

Discussion

Data in the present study indicate that CPC aging conditions myocardial aging and heart failure. Chronological age leads to telomeric shortening in CPCs, which generate a progeny that rapidly acquires the senescent phenotype. Daughter cells inherit the shortened telomeres of maternal CPCs and, after a few rounds of division, express the senescence-associated protein $p16^{INK4a}$. The pool of old cardiomyocytes progressively increases, and ventricular function is impaired. These observations in rats are consistent with findings in humans experiencing aging myopathy.[5,20] Progenitor cell aging af-

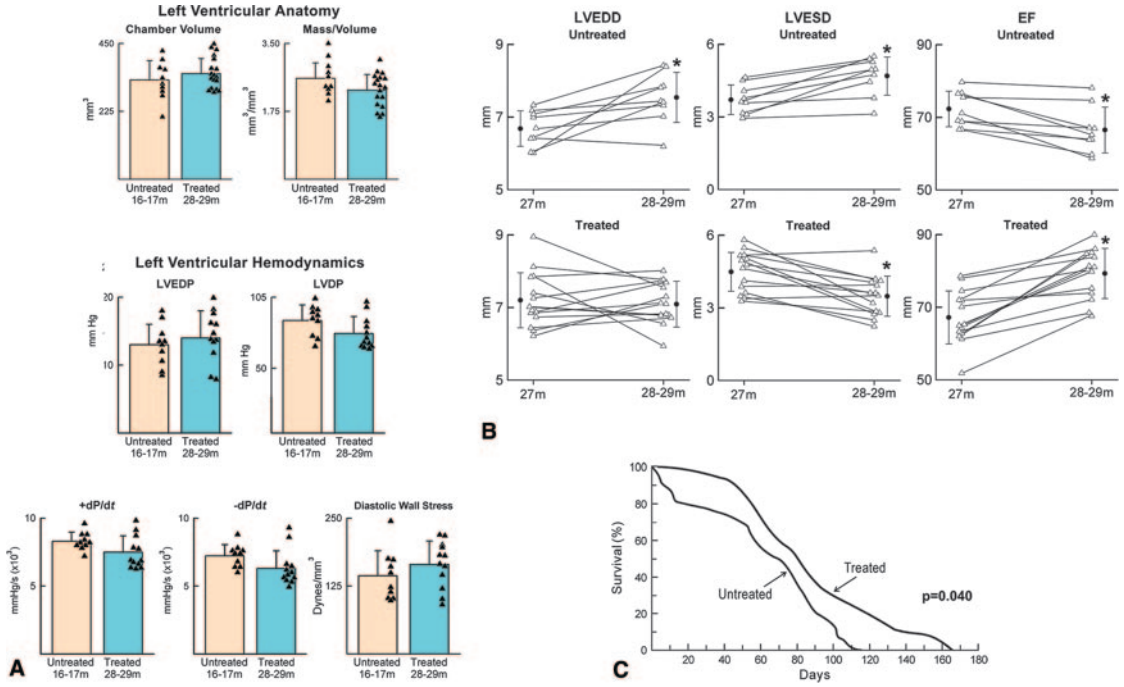

Figure 8. Cardiac function and mortality. A, Anatomy and hemodynamics of untreated hearts at 16 to 17 months and treated hearts at 28 to 29 months. Triangles indicate individual values. B, Echocardiography at baseline at 27 months and 45 days later in the absence and presence of treatment. *$P<0.05$ vs the same hearts at 27 months. C, Mortality in untreated and treated animals at 27 months.

fects the function of the brain, pancreas, and bone marrow,[6] which, together with current results in the heart, point to stem cell dysfunction as a critical determinant of organ and organism aging. However, telomerase-competent CPCs with long telomeres are present in regions of storage in the atria and apex, and following activation by growth factors, migrate to areas of damage, where they create a population of young myocytes, reversing, to some extent, the aging myopathy structurally and functionally. The senescent heart phenotype is partially corrected and the improvement in cardiac performance results in prolongation of maximum lifespan.

The loss of CPC function with aging is mediated partly by an imbalance between factors promoting growth, migration, and survival and factors enhancing oxidative stress, telomere attrition, and death. Three growth-factor receptor systems appear to play a role in the development of CPC senescence and myocardial aging: IGF-1/IGF-1R, HGF/c-Met, and RAS. The IGF-1/IGF-1R induces CPC division, upregulates telomerase activity, hinders replicative senescence, and preserves the pool of functionally competent CPCs.[16,21] The expression of IGF-1R and the synthesis of IGF-1 are attenuated in aging CPCs, diminishing the ability of IGF-1 to activate cell growth and interfere with oxidative damage and telomeric shortening.[22] 8-OH-dG accumulates in old CPCs, favoring telomere dysfunction, cellular senescence, and growth arrest. Additionally, the expression and secretion of HGF in CPCs decreases with age, impacting on their ability to translocate to areas of damage and promote cardiac repair.[23] Defects in these 2 autocrine–paracrine effector pathways may have profound consequences on CPC function and may account for myocyte death, myocardial scarring, and depressed performance of the old heart.[20]

The recognition that a local RAS is present in CPCs and the formation of Ang II is enhanced in old cells provides evidence in favor of the role of this octapeptide in CPC senescence and death. Ang II may contribute to the age-dependent accumulation of oxidative damage in the heart.[24] Inhibition of Ang II function positively interferes with heart failure and prolongs life in humans.[18] Ang II generates reactive oxygen species, and the most prominent form of DNA damage induced by free radicals is 8-OH-dG. In the presence of Ang II, 8-OH-dG increases more in old than in young CPCs. 8-OH-dG accumulates at the GGG triplets of telomeres, resulting in telomeric shortening and uncapping,[19] and loss of telomere integrity is the major determinant of cellular senescence and death. Conversely, IGF-1 interferes with reactive oxygen species generation,[24] decreases oxidative stress with age,[16] and can repair DNA damage by homologous recombination.[25]

The recognition that IGF-1 and HGF modify the effects of aging on CPC behavior, myocardial composition, ventricular performance, and maximum lifespan points to IGF-1 and HGF as potential therapeutic targets of the aging myopathy. Although it is impossible to discriminate the contribution of each growth factor to the reversal of myocardial aging in the rat model, cardiac-restricted overexpression of IGF-1 delays the aging myopathy and the manifestations of heart failure in transgenic mice.[16] These findings are at variance with the notion that IGF-1 promotes premature aging in fruit flies and nematodes.[26] In these lower organisms, attenuation of insulin/IGF-1 signaling prolongs lifespan. However, with adulthood, *Caenorhabditis elegans* and *Drosophila* lose the regenerative capacity of somatic tissues, which makes comparisons with mammals hardly feasible.[27] Dying cells cannot be replaced, and this results in a rapid and progressive decline in organ function. Conversely, cell turnover by activation and commitment of resident progenitor cells remains active in mammals throughout life and IGF-1

potentiates regeneration in susceptible cells. The impact of IGF-1 on terminally differentiated cells is complex and only partially understood. The growth-promoting effects of IGF-1 may be repressed, and metabolic insulin signals may predominate,[28] enhancing oxidative stress and apoptosis.

The modest increase in lifespan of mice heterozygous for the deletion of IGF-1R is restricted to the female cohort, and the lack of evidence in males remains unexplained.[29] Animal models with deficiencies in IGF-1 are complicated by the presence of hypopituitarism, which results in multiple developmental abnormalities.[30] These confounding factors make the dwarf mice inappropriate for the assessment of the role of IGF-1 in biological aging and lifespan.[30] In fact, women live several years more than men, have a reduced incidence of heart failure, and have a better prognosis in the presence of heart failure.[18] The female heart is more resistant to aging than the male heart and has an enhanced expression and nuclear localization of Akt,[31] powerful survival factor and distal effector of IGF-1. Increased levels of IGF-1 characteristically decrease the incidence of heart failure and mortality in the elderly population.[32] Hormone-replacement therapy with restoration of IGF-1 levels has significant health benefits.[30] As suggested by the current results, the effects of IGF-1 on the human heart may involve the CPC compartment potentiating their ability to divide and differentiate. Translation of results in simple postmitotic organisms to mammals in which the life and death of somatic organs is regulated by a stem cell compartment is open to question.

Sources of Funding

This study was supported by NIH grants. A.G. is the recipient of a Norman R. Alpert Visiting Scientist Award from the American Heart Association and the European Society of Cardiology.

Disclosures

None.

References

1. Lakatta EG, Levy D. Arterial and cardiac aging: major shareholders in cardiovascular disease enterprises. Part II: the aging heart in health: links to heart disease. *Circulation*. 2003;107:346–354.
2. Sanderson WC, Scherbov S. Average remaining lifetimes can increase as human populations age. *Nature*. 2005;435:811–813.
3. Bagby GC, Lipton JM, Sloand EM, Schiffer CA. Marrow failure. *Hematology Am Soc Hematol Educ Program*. 2004:318–336.
4. Urbanek K, Torella D, Sheikh F, De Angelis A, Nurzynska D, Silvestre F, Beltrami CA, Bussani R, Beltrami AP, Quaini F, Bolli R, Leri A, Kajstura J, Anversa P. Myocardial regeneration by activation of multipotent cardiac stem cells in ischemic heart failure. *Proc Natl Acad Sci U S A*. 2005;102:8692–8697.
5. Chimenti C, Kajstura J, Torella D, Urbanek K, Heleniak H, Colussi C, Di Meglio F, Nadal-Ginard B, Frustaci A, Leri A, Maseri A, Anversa P. Senescence and death of primitive cells and myocytes lead to premature cardiac aging and heart failure. *Circ Res*. 2003;93:604–613.
6. Beausejour CM, Campisi J. Ageing: balancing regeneration and cancer. *Nature*. 2006;443:404–405.
7. Beltrami AP, Barlucchi L, Torella D, Baker M, Limana F, Chimenti S, Kasahara H, Rota M, Musso E, Urbanek K, Leri A, Kajstura J, Nadal-Ginard B, Anversa P. Adult cardiac stem cells are multipotent and support myocardial regeneration. *Cell*. 2003;114:763–776.
8. Urbanek K, Cesselli D, Rota M, Nascimbene A, De Angelis A, Hosoda T, Bearzi C, Boni A, Bolli R, Kajstura J, Anversa P, Leri A. Stem cell niches in the adult mouse heart. *Proc Natl Acad Sci U S A*. 2006;103:9226–9231.
9. Linke A, Müller P, Nurzynska D, Casarsa C, Torella D, Nascimbene A, Castaldo C, Cascapera S, Böhm M, Quaini F, Urbanek K, Leri A, Hintze TH, Kajstura J, Anversa P. Stem cells in the dog heart are self-renewing, clonogenic and multipotent and regenerate infarcted myocardium, improving cardiac function. *Proc Natl Acad Sci U S A*. 2005;102:8966–8971.
10. Leri A, Kajstura J, Anversa P. Cardiac stem cells and mechanisms of myocardial regeneration. *Physiol Rev*. 2005;85:1373–1416.
11. Tumbar T, Guasch G, Greco V, Blanpain C, Lowry WE, Rendl M, Fuchs E. Defining the epithelial stem cell niche in skin. *Science*. 2004;303:359–363.
12. Kiel MJ, He S, Ashkenazi R, Gentry SN, Teta M, Kushner JA, Jackson TL, Morrison SJ. Haematopoietic stem cells do not asymmetrically segregate chromosomes or retain BrdU. *Nature*. 2007;449:238–242.
13. Wei ZG, Cotsarelis G, Sun TT, Lavker RM. Label-retaining cells are preferentially located in fornical epithelium: implications on conjunctival epithelial homeostasis. *Invest Ophthalmol Vis Sci*. 1995;36:236–246.
14. Braun KM, Niemann C, Jensen UB, Sundberg JP, Silva-Vargas V, Watt FM. Manipulation of stem cell proliferation and lineage commitment: visualisation of label-retaining cells in wholemounts of mouse epidermis. *Development*. 2003;130:5241–5255.
15. Orlic D, Fischer R, Nishikawa S, Nienhuis AW, Bodine DM. Purification and characterization of heterogeneous pluripotent hematopoietic stem cell populations expressing high levels of c-kit receptor. *Blood*. 1993;82:762–770.
16. Torella D, Rota M, Nurzynska D, Musso E, Monsen A, Shiraishi I, Zias E, Walsh K, Rosenzweig A, Sussman MA, Urbanek K, Nadal-Ginard B, Kajstura J, Anversa P, Leri A. Cardiac stem cell and myocyte aging, heart failure, and insulin-like growth factor-1 overexpression. *Circ Res*. 2004;94:514–524.
17. Force T, Krause DS, Van Etten RA. Molecular mechanisms of cardiotoxicity of tyrosine kinase inhibition. *Nat Rev Cancer*. 2007;7:332–344.
18. O'Meara E, Clayton T, McEntegart MB, McMurray JJV, Pina IL, Granger CB, Ostergren J, Michelson EL, Solomon SD, Pocock S, Yusuf S, Swedberg K, Pfeffer MA, CHARM Investigators. Sex differences in clinical characteristics and prognosis in a broad spectrum of patients with heart failure. *Circulation*. 2007;115:3111–3120.
19. Kawanishi S, Oikawa S. Mechanism of telomere shortening by oxidative stress. *Ann N Y Acad Sci*. 2004;1019:278–284.
20. Wei JY. Age and the cardiovascular system. *N Engl J Med*. 1992;327:1735–1739.
21. Davis ME, Hsieh PC, Takahashi T, Song Q, Zhang S, Kamm RD, Grodzinsky AJ, Anversa P, Lee RT. Local myocardial insulin-like growth factor 1 (IGF-1) delivery with biotinylated peptide nanofibers improves cell therapy for myocardial infarction. *Proc Natl Acad Sci U S A*. 2006;103:8155–8160.
22. Kenyon C. The plasticity of aging: insights from long-lived mutants. *Cell*. 2005;120:449–460.
23. Kollet O, Shivtiel S, Chen YQ, Suriawinata J, Thung SN, Kahn J, Spiegel A, Dar A, Samira S, Goichberg P, Kalinkovich A, Arenzana-Seisdedos F, Nagler A, Hardan I, Revel M, Shafritz DA, Lapidot T. HGF, SDF-1, and MMP-9 are involved in stress-induced human CD34$^+$ stem cell recruitment to the liver. *J Clin Invest*. 2003;112:160–169.
24. Kajstura J, Fiordaliso F, Andreoli AM, Li B, Chimenti S, Medow MS, Limana F, Nadal-Ginard B, Leri A, Anversa P. IGF-1 overexpression inhibits the development of diabetic cardiomyopathy and angiotensin II-mediated oxidative stress. *Diabetes*. 2001;50:1414–1424.
25. Yang S, Chintapalli J, Sodagum L, Baskin S, Malhotra A, Reiss K, Meggs LG. Activated IGF-1R inhibits hyperglycemia-induced DNA damage and promotes DNA repair by homologous recombination. *Am J Physiol Renal Physiol*. 2005;289:F1144–F1152.
26. Tatar M, Bartke A, Antebi A. The endocrine regulation of aging by insulin-like signals. *Science*. 2003;299:1346–1351.
27. Maier B, Gluba W, Bernier B, Turner T, Mohammad K, Guise T, Sutherland A, Thorner M, Scrable H. Modulation of mammalian life span by the short isoform of p53. *Genes Dev*. 2004;18:306–319.
28. Dupont J, Holzenberger M. Biology of insulin-like growth factors in development. *Birth Defects Res C Embryo Today*. 2003;69:257–271.
29. Holzenberger M, Dupont J, Ducos B, Leneuve P, Geloen A, Even PC, Cervera P, Le Bouc Y. IGF-1 receptor regulates lifespan and resistance to oxidative stress in mice. *Nature*. 2003;421:182–187.
30. Carter CS, Ramsey MM, Sonntag WE. A critical analysis of the role of growth hormone and IGF-1 in aging and lifespan. *Trends Genet*. 2002;18:295–301.
31. Camper-Kirby D, Welch S, Walker A, Shiraishi I, Setchell KD, Schaefer E, Kajstura J, Anversa P, Sussman MA. Myocardial Akt activation and gender: increased nuclear activity in females versus males. *Circ Res*. 2001;88:1020–1027.
32. Vasan RS, Sullivan LM, D'Agostino RB, Roubenoff R, Harris T, Sawyer DB, Levy D, Wilson PW. Serum insulin-like growth factor 1 and risk for heart failure in elderly individuals without a previous myocardial infarction: the Framingham Heart Study. *Ann Inter Med*. 2003;139:642–648.

Circulation Research
JOURNAL OF THE AMERICAN HEART ASSOCIATION

Activation of Cardiac Progenitor Cells Reverses the Failing Heart Senescent Phenotype and Prolongs Lifespan

Arantxa Gonzalez, Marcello Rota, Daria Nurzynska, Yu Misao, Jochen Tillmanns, Caroline Ojaimi, M. Elena Padin-Iruegas, Patrick Müller, Grazia Esposito, Claudia Bearzi, Serena Vitale, Buddhadeb Dawn, Santosh K. Sanganalmath, Mathue Baker, Thomas H. Hintze, Roberto Bolli, Konrad Urbanek, Toru Hosoda, Piero Anversa, Jan Kajstura and Annarosa Leri

Circ Res. 2008;102:597-606; originally published online January 17, 2008;
doi: 10.1161/CIRCRESAHA.107.165464
Circulation Research is published by the American Heart Association, 7272 Greenville Avenue, Dallas, TX 75231

Print ISSN: 0009-7330. Online ISSN: 1524-4571

Supplemental Data

Supplemental Materials and Methods

Animals

Male Fischer 344 rats were employed because they develop spontaneously heart failure as a function of age.[1-3] At comparables age intervals, ventricular decompensation and structural abnormalities are attenuated in female rats.[4,5] Importantly, a similar behavior has been found in humans.[6] Additionally, aging effects characterized by myocyte loss, myocardial scarring, increased wall stress and impaired myocyte mechanics become apparent in male Fischer 344 rats as early as at 12 months of age.[1-3,7]

Under ketamine (100 mg/kg b.w., i.p.) and acepromazine (1 mg/kg b.w., i.p.) anesthesia and mechanical ventilation, rats at 15, 20 and 27 months of age were injected in the atrioventricular-groove and apex with a retrovirus encoding EGFP. A retrovirus was preferred to a lentivirus to infect only cycling cells. By this approach, it was possible to prevent the activation of the cell cycle in post-mitotic myocytes. Two days later, HGF and IGF-1 (GFs) were delivered intramyocardially. Three injections each were made from the atria and apex to the mid-region of the left ventricle (LV). The concentration of HGF was increased progressively towards the LV mid-region while the amount of IGF-1 was maintained constant (supplemental Figure XIII). Control animals of the same age were injected with the EGFP-retrovirus and then with vehicle. BrdU was given in the drinking water (1 mg/ml) throughout the experiments to label newly formed cells. Animals were studied 45 days later.

Ventricular Function and Anatomy

Before sacrifice, hemodynamic parameters were obtained in rats non-injected, injected with vehicle (untreated) or with GFs (treated). Animals were anesthetized with chloral hydrate (300 mg/kg b.w., i.p.), and the right carotid artery was cannulated with a microtip pressure transducer (SPR-612, Millar Instruments) connected to an A/D converter (iWorx 214) and a computer system. The catheter was advanced into the LV chamber for the evaluation of LV end-diastolic pressure (LVEDP), systolic pressure (LVSP), developed

pressure (LVDP) and + and − dP/dt in the closed-chest preparation.[1-3,8-10] Wall thickness measurements in combination with the radius of the LV chamber (see below) and LVEDP were employed to compute diastolic wall stress.

Following the collection of hemodynamic measurements, the abdominal aorta was cannulated with a polyethylene catheter filled with phosphate buffer (0.2 mol/L, pH 7.4) and heparin (100 IU/ml). In rapid succession, the heart was arrested in diastole by injection of cadmium chloride (100 mmol/L) through the aortic catheter and perfusion with phosphate buffer was conducted for ~3 minutes. The thorax was opened and the right atrium was cut to allow drainage of blood and perfusate. The heart was then fixed by perfusion with 10% phosphate-buffered formalin. Perfusion pressure was adjusted to mean arterial pressure. Throughout the procedure, the LV chamber was filled with fixative from a pressure reservoir set at a height equivalent to the in vivo measured end-diastolic pressure.[1-3,8-10] After fixation, the heart was dissected and the weights of the right ventricle and LV inclusive of the interventricular septum were recorded. The major longitudinal axis from the base to the apex of the heart was determined and the LV was serially sectioned into five rings perpendicular to this axis. The minimal and maximal cavitary diameters and wall thickness at the mid-region of the ventricle were obtained and, together with the longitudinal axis, were utilized to compute LV chamber volume.[11,12] Magnitude of sampling is listed in supplemental Table I.

Echocardiography

Echocardiograms were recorded in rats at 27 months before treatment with GFs and 45 days later after the injection of GFs at 28-29 months. A group of rats injected with vehicle was similarly studied. Rats were anesthetized with ketamine (100 mg/kg b.w., i.p.), and echocardiographic parameters were collected utilizing an Acuson Sequoia 256c equipped with a 13-MHz linear transducer.[11,12] The anterior chest was shaved, and rats were placed in the left lateral decubitus position. A rectal temperature probe was placed, and the body temperature was carefully maintained between 37.0°C and 37.5°C with a heating pad throughout the study. The parasternal long-axis, parasternal short-axis, and

apical four-chamber views were used to obtain 2D, M-mode. Systolic and diastolic anatomic parameters were obtained from M-mode tracings at the midpapillary level. Ejection fraction (EF) was calculated by the area-length method.[11,12]

CPC Number

This analysis was restricted to c-kit-positive-CPCs in the atria, base-mid-region and apex of the LV in rats at 4, 12, 20 and 28 months of age. CPCs were identified by employing an antibody against c-kit (R&D Systems). Cell phenotype was defined by immunocytochemistry. CPCs were tested for markers of cardiac, skeletal muscle, neural and hematopoietic cell lineages to detect Lin^{neg}-CPCs.[9,10,12] To recognize myocyte progenitors and precursors the presence of c-kit together with transcription factors and cytoplasmic proteins specific of myocytes was determined. A complete list of antibodies used is shown in supplemental Table II.

Morphometric measurements of CPCs, myocyte progenitors and myocyte precursors were obtained by counting at confocal microscopy the number of CPCs or the two other cell categories per unit area, N(cpc)A, of LV and atrial myocardium. Additionally, the number of CPCs per unit volume of myocardium, N(cpc)V, and the average diameter of CPCs, D(cpc), were obtained utilizing the Schwartz-Saltykov methodology.[13-15] An identical approach was followed for the measurements of myocyte progenitors and precursors. Additionally, the number of CPCs that reached replicative senescence and irreversible growth arrest[16-18] was evaluated by the expression of the senescence-associated protein $p16^{INK4a}$. Also, the fraction of CPCs undergoing apoptosis[12,14,19] was evaluated by the hairpin 1 to establish the number of functionally-competent CPCs[14,20] in the various anatomical areas of the heart with aging. An identical approach was followed to analyze aging effects on the number of CPCs which expressed IGF-1 and IGF-1R, HGF and c-Met, and Ang II and AT1 receptors.

Long-Term BrdU-Retaining Assay

Rats at 4 and 27 months were divided in two groups each. In the first case, rats at 4 and 27 months were exposed to BrdU in the drinking water for 7 days and subsequently were

sacrificed and studied. In the second case, rats at 4 and 27 months were exposed to BrdU in the drinking water for 7 days and studied after a chasing period of 12 weeks, at 7 and 30 months, respectively. Nearly 70% of the old animals died during the chase-period. This reflected the anticipated death rate of male Fischer 344 rats at this age. Unfortunately, death occurred mostly during the night and the organs deteriorated rapidly after death. This limitation made the identification of the cause of death essentially impossible. BrdU-bright and BrdU-dim c-kit-positive-CPCs were counted at both time points in both young and old rats. Levels of fluorescence >4,000 and <2,000 units (pixel x average intensity) were considered representative of bright and dim cells, respectively.[15] CPCs with intermediate levels of fluorescence, >2,000 but <4,000, were excluded from the analysis.

These criteria were introduced to score the long-term label-retaining CPCs.[15] The autofluorescence of the section, together with the signal generated by the irrelevant antibody used as a negative control for BrdU staining, was <60 units. Levels of labeling >200 units were included. BrdU-negative-CPCs were also counted. An identical approach was used to evaluate the fraction of myocyte nuclei labeled by bright and dim BrdU at 7 days and after 12 weeks of chasing. However, myocyte nuclei with intermediate fluorescence intensity (>2,000 and <4,000) were included in the analysis to obtain a complete evaluation of the generated myocyte progeny over a period of 12 weeks.[15] The myocyte mitotic index[15,20] was also measured by the expression of phospho-H3 in young and old hearts to have a quantitative estimate of the actual population of amplifying myocytes in the LV myocardium.[10,21]

Isolation and Growth Properties of CPCs

The heart was dissected, the aorta was removed and the LV myocardium was cut into small pieces and incubated in a collagenase solution.[9,12] The fraction of small cells was enriched by filtration and centrifugation and c-kit-positive-cells were sorted for c-kit with rabbit anti-c-kit (Santa Cruz Biotechnology) and magnetic immunobeads (Miltenyi). Cell phenotype was defined by immunocytochemistry. Therefore, the separated c-kit-positive-

cells were fixed in 4% paraformaldehyde for 15 minutes at room temperature and tested for multiple markers (supplemental Table II) to detect Lin^{neg}-CPCs.[9,12,15,20] Committed cells expressed the stem cell antigens c-kit, MDR1 or Sca-1 alone or in combination together with transcription factors and cytoplasmic proteins of cardiac cells. The growth of CPCs was determined by BrdU labeling and population doubling time. Cells were labeled with BrdU (1 μg/ml, Roche) for 5 days and BrdU incorporation was determined by immunostaining with monoclonal antibody (Roche). For studies of growth kinetics, the number of cells per unit area was counted daily and the data were plotted on a semi-logarithmic scale. Population doubling time was calculated by linear regression analysis.

Immunocytochemistry

Formalin-fixed tissue sections, 4 μm in thickness, were employed for these studies. When possible, antibodies were directly labeled with fluorochromes (Molecular Probes) or quantum dots (Quantum Dot Corporation) to avoid cross-reactivity and autofluorescence (supplemental Table II).[22,23]

Telomerase Activity and Telomere Length

Expanded (passage P7-P8) c-kit-positive-CPCs from hearts at 3 and 27 months were homogenized in CHAPS buffer and centrifuged at 4°C. Untreated and RNase-treated cell extracts were incubated with [γ-^{32}P]ATP-end-labeled telomerase substrate (TS oligonucleotide: 5'-AATCCGTCGA-GCAGAGTT-3'), Taq polymerase and anchored reverse primer (5'-GCGCGC-[CTAACC]$_3$CTAACC-5') for 45 min. Samples were exposed to 28 amplification cycles.[20,24,25] PCR products were separated on 12% polyacrylamide gel. Telomerase-induced reaction generated a 6-bp ladder. The optical density (OD) of the bands was normalized for PCR efficiency.

Telomere length was evaluated in cytospins of freshly isolated c-kit-positive-cells from hearts at 3 and 27 months by quantitative fluorescence in situ hybridization (Q-FISH) and confocal microscopy.[20,26,27] Similarly, telomere length was evaluated in small developing myocytes in tissue sections of young and old hearts. A fluorescein isothiocyanate-peptide nucleic acid (FITC-PNA) probe was used. The fluorescent signals

measured in lymphoma cells with short (L5178Y-S, 7 kbp) and long (L5178Y-R, 48 kbp) telomeres (kindly provided by Dr. M.A. Blasco, Spanish National Cancer Centre, Madrid) were utilized to compute absolute telomere length.

CPC Proliferation and Death

C-kit-positive-CPCs from hearts at 3 and 27 months at P7-P8 were cultured in SFM and stimulated with IGF-1 (150 ng/mL), HGF (200 ng/mL), IGF-1 and HGF together (IGF-1-HGF) or Ang II (10^{-9}mol/L) for 24 hours. BrdU was added to the medium at 8 hour intervals. Cells were fixed and BrdU incorporation was measured as previously described.[9,10,12] In a similar manner, CPCs were stimulated with Ang II (10^{-9}mol/L) alone or in the presence of IGF-1 (150 ng/mL), HGF (200 ng/mL) and IGF-1-HGF for 24 hours. Cells were fixed and apoptosis was determined by the TdT assay.[3,14] The effect of Ang II (10^{-9}M) for 24 hours on the extent of oxidative stress in CPCs was measured by the presence of 8-OH-dG.[14] The intensity of the 8-OH-dG signal was measured with an ImagePro software[19,25] and normalized for the PI fluorescence.

ELISA

Expanded c-kit-positive-CPCs from hearts at 3 and 27 months (P5-P6) were cultured in SFM and exposed to IGF-1 (150 ng/mL), HGF (200 ng/mL) or Ang II (10^{-11}mol/L) for a period of 24 hours. Media containing GFs were removed and cells were washed twice and fresh SFM was added. The SFM contained antibodies against IGF-1R (Abcam) and c-Met (R&D Systems) or the AT1 receptor antagonist telmisartan (10^{-7}mol/L; Sigma) and the AT2 receptor blocker PD123319 (10^{-7}mol/L, Sigma). The blockers were employed to avoid ligand binding. Media were collected after 3 and 9 hours for IGF-1, HGF and Ang II. GF quantities were determined by ELISA (IGF-1, R&D Systems; HGF, B-Bridge International; Ang II, Peninsula Laboratories) and normalized by the total quantity of CPC proteins and β-actin (Sigma) expression measured by Western blotting.

Real-Time RT-PCR

Total RNA was extracted from c-kit-positive-CPCs obtained from hearts at 3, 12, 16 and 24 months with a commercial RNA isolation kit using Trizol (TRI REAGENT, Sigma) as described previously in detail.[28] cDNA was obtained from 500 ng total RNA in a 20 μl reaction containing first strand buffer, 0.4 mM each of dTTP, dATP, dGTP and dCTP together with 200U of Superscript III (Invitrogen), 10U of RNase inhibitor (RNasin Plus, Promega) and 500 ng of random hexamer (Promega). This mixture was incubated at 42ºC for 2 hours. Subsequently, real-time RT-PCR was performed with primers (supplemental Table III) designed using the Primer Express v2.0 analysis software (Applied Biosystems). The LightCycler PCR system (Roche Diagnostics) was employed for real-time RT-PCR that was done in duplicates. In each case, 5 ng cDNA were used with the exception of renin that required 15 ng. cDNA was combined with SYBR Green master mix (LightCycler Fast Start DNA Master SYBR Green I, Roche) and cycling conditions were as follows: 95°C for 10 min followed by 45 cycles of amplification (95°C denaturation for 10 sec, annealing for 5 sec and 72°C extension for 20 sec). The melting curve was then obtained. The annealing temperature used for each primer set is listed in supplemental Table III. To avoid the influence of genomic contamination, forward and reverse primers for each gene were located in different exons. Reactions containing cDNA generated without reverse transcriptase and reactions with primers alone were also included. PCR efficiency was evaluated using a standard curve of four serial dilution points. Quantified values were normalized against the input determined by the housekeeping gene β-actin.

Real-time PCR products were run on 1.8% agarose/1x TBE gel. Amplified fragments were cut out and DNA was extracted using QIAquick Gel Extraction kit (Qiagen). DNA was eluted in 30 μl of 10 mmol/L Tris buffer (pH 8.5), and amplified by Platinum Blue PCR Supermix (Invitrogen) in the presence of 260 nmol/L of the forward and reverse primers utilized for real-time PCR. PCR reaction was carried out in Eppendorf Mastercycler. Cycling conditions were as follows: 94°C for 2 min followed by

35 cycles of amplification (94°C denaturation for 20 sec, annealing for 30 sec, 72°C elongation for 20 sec) with a final incubation at 72°C for 3 min. After purification using QIAquick PCR Purification kit (Qiagen), samples were submitted to the DNA Sequencing Facility of Cornell University (New York, NY) to obtain the DNA sequence.

Western Blotting

Proteins from expanded CPCs (P5-P6) obtained from hearts at 3 and 27 months were extracted using M-PER Mammalian Protein Extraction Reagent (Pierce Biotechnology) and a cocktail of protease inhibitors (Pierce Biotechnology). Protein concentration was measured by Bradford assay (Bio-Rad). Equivalents of 30 μg protein for Aogen and AT1 receptor were separated on 8% SDS-PAGE. Proteins were then transferred onto nitrocellulose membranes, blocked with 5% BSA (AT1 receptor) or 5% dry skim milk (Aogen) in Tris-saline buffer with 0.1% Tween20 (TBST) for 1 h at room temperature, and exposed to mouse-monoclonal Aogen antibody (Swant) 1/1000 or to mouse-monoclonal AT1 receptor antibody (Abcam) 1/500 in TBST overnight at 4ºC. HRP-conjugated IgG were used as secondary antibodies (Pierce Biotechnology). Proteins were detected by chemiluminescence (SuperSignal West Femto Maximum Sensitivity Substrate, Pierce Biotechnology) and OD was measured.[10,19] Loading conditions were determined by the expression of β-actin (Sigma).

Cell Migration

These studies were restricted to rats at 4 and 27 months. A retrovirus encoding EGFP was injected in the atrioventricular-groove to label cycling CPCs (supplemental Figure IV).[10] Two days later, GFs or vehicle were injected and the heart was excised, arrested in diastole with 30 mmol/L KCl and placed in a bath mounted on the stage of a two-photon microscope (Bio-Rad Radiance 2100MP). The heart was continuously perfused retrogradely through the aorta and superfused at 37°C with an oxygenated Tyrode solution in the absence or presence of rhodamine-labeled dextran. Dextran has a molecular weight of 70,000 and because of this size, dextran does not cross the endothelial barrier and remains confined to the coronary vasculature.[10,11] EGFP and

rhodamine were excited, respectively, at 960 and 840 nm with mode-locked Ti:Sapphire femtosecond laser (Tsunami, Spectra-Physics). The corresponding images were acquired at emission wavelengths of 515 and 600 nm. By this approach, the translocation of EGFP-positive-cells and their localization with respect to the coronary vasculature was determined over time.[10] Subsequently, hearts were fixed and analyzed by confocal microscopy as discussed above.

Data Analysis and Statistics

The magnitude of sampling utilized in each in vitro and in vivo determination is listed in supplemental Table I. In all cases, results are presented as mean±SD. Significance between two comparisons was determined by unpaired and paired Student's *t*-test and among multiple comparisons by Bonferroni test. Mortality was measured by log-rank test. All *P* values are two-sided and $P<0.05$ was considered to be significant.

References

1. Anversa P, Palackal T, Sonnenblick EH, Olivetti G, Meggs LG, Capasso JM. Myocyte cell loss and myocyte cellular hyperplasia in the hypertrophied aging rat heart. *Circ Res.* 1990;67:871-885.

2. Capasso JM, Palackal T, Olivetti G, Anversa P. Severe myocardial dysfunction induced by ventricular remodeling in aging rat hearts. *Am J Physiol.* 1990;259:H1086-H1096.

3. Kajstura J, Cheng W, Sarangarajan R, Li P, Li B, Nitahara JA, Chapnick S, Reiss K, Olivetti G, Anversa P. Necrotic and apoptotic myocyte cell death in the aging heart of Fischer 344 rats. *Am J Physiol*. 1996;271:H1215-H1228.

4. Forman DE, Cittadini A, Azhar G, Douglas PS, Wei JY. Cardiac morphology and function in senescent rats: gender-related differences. *J Am Coll Cardiol.* 1997;30:1872-1877.

5. Leri A, Kajstura J, Li B, Sonnenblick EH, Beltrami CA, Anversa P, Frishman WH. Cardiomyocyte aging is gender-dependent: the local IGF-1-IGF-1R system. *Heart Dis.* 2000;2:108-115.

6. Olivetti G, Giordano G, Corradi D, Melissari M, Lagrasta C, Gambert SR, Anversa P. Gender differences and aging: effects on the human heart. *J Am Coll Cardiol.* 1995;26:1068-1079.

7. Capasso JM, Fitzpatrick D, Anversa P. Cellular mechanisms of ventricular failure: myocyte kinetics and geometry with age. *Am J Physiol.* 1992;262:H1770-H1781.

8. Leri A, Claudio PP, Li Q, Wang X, Reiss K, Wang S, Malhotra A, Kajstura J, Anversa P. Stretch-mediated release of angiotensin II induces myocyte apoptosis by activating p53 that enhances the local renin-angiotensin system and decreases the Bcl-2-to-Bax protein ratio in the cell. *J Clin Invest*. 1998;101:1326-1342.

9. Beltrami AP, Barlucchi L, Torella D, Baker M, Limana F, Chimenti S, Kasahara H, Rota M, Musso E, Urbanek K, Leri A, Kajstura J, Nadal-Ginard B, Anversa P. Adult cardiac stem cells are multipotent and support myocardial regeneration. *Cell*. 2003;114:763-776.

10. Urbanek K, Rota M, Cascapera S, Bearzi C, Nascimbene A, De Angelis A, Hosoda T, Chimenti S, Baker M, Limana F, Nurzynska D, Torella D, Rotatori F, Rastaldo R, Musso E, Quaini F, Leri A, Kajstura J, Anversa P. Cardiac stem cells possess growth factor-receptor systems that after activation regenerate the infarcted myocardium, improving ventricular function and long-term survival. *Circ Res*. 2005;97:663-673.

11. Dawn B, Stein AB, Urbanek K, Rota M, Whang B, Rastaldo R, Torella D, Tang XL, Rezazadeh A, Kajstura J, Leri A, Hunt G, Varma J, Prabhu SD, Anversa P, Bolli R. Cardiac stem cells delivered intravascularly traverse the vessel barrier, regenerate infarcted myocardium, and improve cardiac function. *Proc Natl Acad Sci USA*. 2005;102:3766-3771.

12. Linke A, Müller P, Nurzynska D, Casarsa C, Torella D, Nascimbene A, Castaldo C, Cascapera S, Böhm M, Quaini F, Urbanek K, Leri A, Hintze TH, Kajstura J, Anversa P. Stem cells in the dog heart are self-renewing, clonogenic and multipotent and regenerate infarcted myocardium, improving cardiac function. *Proc Natl Acad Sci USA*. 2005;102:8966-8971.

13. Anversa P, Olivetti G. Cellular basis of physiological and pathological myocardial growth. In: Page E, Fozzard HA, Solaro RJ, eds. *Handbook of Physiology*. New York: Oxford Univ. Press; 2002:75-144.

14. Rota M, LeCapitaine N, Hosoda T, Boni A, De Angelis A, Padin-Iruegas ME, Esposito G, Vitale S, Urbanek K, Casarsa C, Giorgio M, Lüscher TF, Pelicci PG, Anversa P, Leri A, Kajstura J. Diabetes promotes cardiac stem cell aging and heart failure, which are prevented by deletion of the p66shc gene. *Circ Res*. 2006;99:42-52.

15. Urbanek K, Cesselli D, Rota M, Nascimbene A, De Angelis A, Hosoda T, Bearzi C, Boni A, Bolli R, Kajstura J, Anversa P, Leri A. Stem cell niches in the adult mouse heart. *Proc Natl Acad Sci USA*. 2006;103:9226-9231.

16. Janzen V, Forkert R, Fleming HE, Saito Y, Waring MT, Dombkowski DM, Cheng T, DePinho RA, Sharpless NE, Scadden DT. Stem-cell ageing modified by the cyclin-dependent kinase inhibitor p16INK4a. *Nature*. 2006;443:421-426.

17. Molofsky AV, Slutsky SG, Joseph NM, He S, Pardal R, Krishnamurthy J, Sharpless NE, Morrison SJ. Increasing p16INK4a expression decreases forebrain progenitors and neurogenesis during ageing. *Nature*. 2006;443:448-452.

18. Krishnamurthy J, Ramsey MR, Ligon KL, Torrice C, Koh A, Bonner-Weir S, Sharpless NE. p16INK4a induces an age-dependent decline in islet regenerative potential. *Nature*. 2006;443:453-457.

19. Kajstura J, Fiordaliso F, Andreoli AM, Li B, Chimenti S, Medow MS, Limana F, Nadal-Ginard B, Leri A, Anversa P. IGF-1 overexpression inhibits the development of

diabetic cardiomyopathy and angiotensin II-mediated oxidative stress. *Diabetes*. 2001;50:1414-1424.

20. Urbanek K, Torella D, Sheikh F, De Angelis A, Nurzynska D, Silvestre F, Beltrami CA, Bussani R, Beltrami AP, Quaini F, Bolli R, Leri A, Kajstura J, Anversa P. Myocardial regeneration by activation of multipotent cardiac stem cells in ischemic heart failure. *Proc Natl Acad Sci USA*. 2005;102:8692-8697.

21. Anversa P, Kajstura J, Leri A, Bolli R. Life and death of cardiac stem cells: a paradigm shift in cardiac biology. *Circulation*. 2006;113:1451-1463.

22. Leri A, Kajstura J, Anversa P. Cardiac stem cells and mechanisms of myocardial regeneration. *Physiol Rev*. 2005;85:1373-1416.

23. Anversa A, Leri A, Rota M, Hosoda T, Bearzi C, Urbanek K, Kajstura J, Bolli R. Concise review: stem cells, myocardial regeneration, and methodological artifacts. *Stem Cells*. 2007;25:589-601.

24. Leri A, Barlucchi L, Limana F, Deptala A, Darzynkiewicz Z, Hintze TH, Kajstura J, Nadal-Ginard B, Anversa P. Telomerase expression and activity are coupled with myocyte proliferation and preservation of telomeric length in the failing heart. *Proc Natl Acad Sci USA*. 2001;98:8626-8631.

25. Torella D, Rota M, Nurzynska D, Musso E, Monsen A, Shiraishi I, Zias E, Walsh K, Rosenzweig A, Sussman MA, Urbanek K, Nadal-Ginard B, Kajstura J, Anversa P, Leri A. Cardiac stem cell and myocyte aging, heart failure, and insulin-like growth factor-1 overexpression. *Circ Res*. 2004;94:514-524.

26. Chimenti C, Kajstura J, Torella D, Urbanek K, Heleniak H, Colussi C, Di Meglio F, Nadal-Ginard B, Frustaci A, Leri A, Maseri A, Anversa P. Senescence and death of primitive cells and myocytes lead to premature cardiac aging and heart failure. *Circ Res*. 2003;93:604-613.

27. Leri A, Franco S, Zacheo A, Barlucchi L, Chimenti S, Limana F, Nadal-Ginard B, Kajstura J, Anversa P, Blasco MA. Ablation of telomerase and telomere loss leads to cardiac dilatation and heart failure associated with p53 upregulation. *EMBO J*. 2003;22:131-139.

28. Ojaimi C, Li W, Kinugawa S, Post H, Csiszar A, Pacher P, Kaley G, Hintze TH. Transcriptional basis for exercise limitation in male eNOS-knockout mice with age: heart failure and the fetal phenotype. *Am J Physiol*. 2005;289:H1399-H1407.

Supplemental Figures

Figure I. CPC senescence and death. **A**, CPCs/mm3 myocardium. **B**, Cluster of c-kit-positive CPCs (green) in the LV at 20 months. Several CPCs express the senescence-associated protein $p16^{INK4a}$ (white; arrowheads). Myocytes, MHC (red). Propidium iodide (PI, blue). Fraction of $p16^{INK4a}$-positive-CPCs (lower panel). **C**, Percentage (upper panel) and number/mm^3 myocardium (lower panel) of apoptotic CPCs. **D**, Functionally-competent CPCs/mm3 myocardium (lower panel). **E**, Myocyte progenitors and precursors. *P<0.05 versus 4 months (4m); **P<0.05 versus 12 months (12m); †P<0.05 versus 20 months (20m).

Figure II. CPC and myocyte formation. **A**, Old LV myocardium containing BrdU (yellow) bright- (arrows), and dim- (arrowhead) myocytes (α-SA, red) at 7 days. Several non-myocyte nuclei are also labeled by BrdU. Negative control (lower panel): LV myocardium from a rat at 28 months of age not exposed to BrdU. **B**, Metaphase chromosomes (upper panels: blue, PI; arrows) positive for phospho-H3 (lower panels: green) are apparent in small dividing cardiomyocytes (α-SA, red) in LV myocardium of young (left panels) and old (right panels) hearts.

Figure III. Telomere length and replicating myocytes. Young (**A**) and old (**B**) LV myocardium contains small cycling (Ki67, yellow; arrows) myocytes with long (**A**) and short (**B**) telomeres.

Figure IV. Growth factor receptor systems in CPCs. Freshly isolated CPCs from young (**A**, **B**, **D**, **E**) and old (**C**, **F**) hearts express IGF-1R (**A**, magenta), c-Met (**B**, yellow) and AT1 receptors (**C**, white) on the membrane and IGF-1 (**D**, magenta), HGF (**E**, yellow) and Ang II (**F**, white) in the cytoplasm.

Figure V. Nucleotide sequences. Sequences of the real-time RT-PCR products were established in sense and antisense direction.

Figure VI. Growth factor treatment. **A**, Schematically, clusters of CPCs are stored in the atria. This anatomical area was injected with EGFP-retrovirus to infect cycling CPCs. Two days after infection, increasing concentrations of HGF alone or together with IGF-1 were delivered intramyocardially from the atria to the LV mid-region to create a chemotactic gradient promoting the migration of CPCs-ECCs. **B**, Section of atrial myocardium containing several CPCs (c-kit, white) some of which were infected by the EGFP-retrovirus (green; arrows). Myocytes (MHC, red).

Figure VII. Migration of EGFP-positive-cells. **A** through **E**, Two days after the injection of the retrovirus, growth factors were administrated and the migration of EGFP-positive-cells was examined ex vivo in an oxygenated Tyrode solution preparation by two-photon microscopy. These images correspond to cell locomotion 10 hours after the administration of growth factors in a Fischer 344 rat at 4 months of age. These five panels, panel C is shown twice, illustrate the same field examined at intervals of 20 minutes each. Green fluorescence reflects EGFP-labeled-cells in vivo. Arrowheads of various colors point to cells moving in the direction of the large open arrows over a period of 80 minutes. The white circle shows cells that appeared in the field and then disappeared. The white small square in panel E shows two cells that began to appear in panel D.

Figure VIII. Identity of the migrated EGFP-positive-cells. Panel **E** in supplemental Figure VII is illustrated again here (**A**). The square defines the EGFP positive cells detected in the living tissue by two-photon microscopy and after fixation and staining of the same LV region by confocal microscopy, panel **B**. Green fluorescence in both panels

identifies the same cells (**A** and **B**). EGFP-positive-cells express c-kit (**C**, green), MDR1 (**D**, yellow), GATA-4 (**C**, white) and c-Met (**E**, red). For example, 3 EGFP-positive-cells are Ki67-positive (**D**, magenta; asterisks) and express c-kit, MDR1 and c-Met (arrowheads) and 1 EGFP-positive-cell expresses all four proteins (arrow). Myocytes (MHC, red). Nuclei (PI, blue).

Figure IX. Migration of EGFP-positive-cells. **A** through **E**, These images correspond to cell locomotion 10 hours after the administration of growth factors in a Fischer 344 rat at 27 months of age. These five panels, panel C is shown twice, illustrate the same field examined at intervals of 15 minutes each. Green fluorescence reflects EGFP-labeled-cells in vivo. Arrowheads of various colors point to cells moving in the direction of the large open arrows over a period of 60 minutes. The red circle shows a cell that was in the field and then disappeared. The yellow oval surrounds cells that moved within the field throughout the period of observation.

Figure X. Identity of the migrated EGFP-positive-cells. Panel **E** in supplemental Figure IX is illustrated again here at higher magnification (**A**). **A**, **B**, Squares and rectangles define the EGFP positive cells detected in the living tissue by two-photon microscopy (**A**) and after fixation and staining of the same LV region by confocal microscopy (**B**). Green fluorescence in both panels identifies the same cells (**A** and **B**). EGFP-positive-cells express c-kit (**C**, green), Sca-1 (**D**, yellow), GATA-4 (**C**, white) and c-Met (**E**, red). For example, 7 EGFP-positive-cells express c-kit, Sca-1 and c-Met (arrowheads) and 3 EGFP-positive-cell express all four proteins (arrows). Myocytes (MHC, red). Nuclei (PI, blue).

Figure XI. Pattern of migration of CPCs. These images were obtained in a Fischer 344 rat at 4 months of age. The coronary circulation was perfused with an oxygenated Tyrode solution containing rhodamine-labeled dextran and the growth factors were administrated at the time of observation. The first image was obtained within 15 minutes, which is the time required for the adjustment of the microscope on the epicardial surface of the heart. **A** through **E**, These five panels, panel **C** is shown twice, illustrate the same field

examined at intervals of 20 minutes each. Red fluorescence corresponds to the distribution of the coronary vasculature and green fluorescence reflects EGFP-labeled cells in vivo. Arrowheads of various colors point to EGFP-positive cells moving in the direction of the large open arrows over a period of 80 minutes. In all panels, EGFP moving cells were outside of the coronary vessels, suggesting that the coronary circulation was not implicated in the migration of EGFP-positive cells (color arrowheads) within the myocardium. **F**, Migrating EGFP-positive cells were located within tunnels defined by interstitial fibronectin (yellow). Large arrows point to the direction of migration of the EGFP-positive cells.

Figure XII. Cell migration and cardiac aging. **A**, Properties of migrating EGFP-positive-cells in young (4m) and old (27m) hearts with growth factors. **P*<0.05 versus 4 months. Telomere length (**B** and **C**; magenta) in migrating (**B**) and non-migrating (**C**) CPCs. Migrating CPCs are $p16^{INK4a}$-negative (**D**). Non-migrating CPCs are mostly $p16^{INK4a}$-positive (**E**).

Figure XIII. Growth factor treatment. Schematically, clusters of CPCs are stored in the atria and apex. These anatomical areas were injected with an EGFP-retrovirus to infect cycling CPCs and ECCs. Two days after infection, increasing concentrations of HGF together with IGF-1 were delivered intramyocardially from the atria and apex to the LV mid-region. The objective was to create a chemotactic gradient between stored CPCs and the damaged myocardium to promote translocation of functionally-competent primitive cells to the areas of tissue injury. Control animals were injected with vehicle. Treated and untreated animals were examined 45 days later.

Figure XIV. Myocyte and coronary vessel regeneration. **A**, Newly formed EGFP-positive-cardiomyocytes (left panel: EGFP, green; right panel: MHC, red; arrows). **B** and **C**, Newly formed EGFP-positive capillaries (**B**, upper panel: EGFP, green; central panel: vWF, white; lower panel: merge) and arterioles (**C**, upper panel: EGFP, green; central

panel: α-SMA, red; lower panel: merge). Treated hearts at 16-17m (**A**), 21-22m (**B**) and 28-29m (**C**). **D**, *P<0.05 versus 16-17 and 21-22 months.

Figure XV. Vessel regeneration. BrdU-positive arterioles and capillaries. *P<0.05 versus 16-17 months. **P<0.05 versus 21-22 months and †P<0.05 versus untreated animals.

Figure XVI. Cardiac anatomy. LV anatomy at baseline (white bars) and 45 days later in untreated (orange bars) and treated (blue bars) rats. *P<0.05 versus baseline and †P<0.05 versus untreated-animals.

Figure XVII. Echocardiography. M-mode echocardiography of rats at 27 months and 45 days later in the absence (**A**) and presence (**B**) of growth factor treatment. The improvement in cardiac performance with treatment is apparent.

Supplemental Movies

Movie I, II. Echocardiographic recordings. Two examples of the positive changes in function with growth factor treatment.

Supplemental TABLE I: Magnitude of Sampling

Parameter	n	Aggregate	Mean±SD
Number of CPCs, Myocyte Progenitors and Precursors			
4 months			
Atria	6	215[(1)]	36±11
Base-Mid	6	863[(1)]	144±20
Apex	6	392[(1)]	65±16
12 months			
Atria	6	229[(1)]	38±6
Base-Mid	6	761[(1)]	127±18
Apex	6	391[(1)]	65±12
20 months			
Atria	6	201[(1)]	34±7
Base-Mid	6	913[(1)]	152±19
Apex	6	446[(1)]	74±15
28 months			
Atria	6	233[(1)]	39±5
Base-Mid	6	765[(1)]	128±16
Apex	6	321[(1)]	54±13
Fraction of $p16^{INK4a}$-Positive CPCs			
4 months			
Atria	6	643[(1)]	107±34
Base-Mid	6	2580[(1)]	430±57
Apex	6	1177[(1)]	196±47
12 months			
Atria	6	458[(1)]	76±12
Base-Mid	6	1523[(1)]	254±37
Apex	6	782[(1)]	130±24

20 months			
Atria	6	402[(1)]	67±14
Base-Mid	6	1822[(1)]	304±38
Apex	6	888[(1)]	148±30
28 months			
Atria	5	384[(1)]	77±9
Base-Mid	5	1292[(1)]	258±35
Apex	5	545[(1)]	109±29
Fraction of Apoptotic CPCs			
4 months			
Atria	6	926[(1)]	154±62
Base-Mid	6	4606[(1)]	768±203
Apex	6	1089[(1)]	182±50
12 months			
Atria	6	615[(1)]	103±11
Base-Mid	6	2843[(1)]	474±48
Apex	6	834[(1)]	139±45
20 months			
Atria	6	371[(1)]	62±16
Base-Mid	6	1185[(1)]	198±37
Apex	6	412[(1)]	69±14
28 months			
Atria	5	243[(1)]	49±10
Base-Mid	5	699[(1)]	140±34
Apex	5	275[(1)]	55±12
Pulse-Chase BrdU Labeling			
4 months CPC pulse	5	1761[(2)]	352±64
4 months CPC chase	5	2887[(2)]	577±216
27 months CPC pulse	5	2726[(2)]	545±121

27 months CPC chase	5	2425[(2)]	485±110
4 months Myocytes pulse	5	8967[(2)]	1793±613
4 months Myocytes chase	5	3541[(2)]	708±213
27 months Myocytes pulse	5	1831[(2)]	366±74
27 months Myocytes chase	5	1187[(2)]	237±29
Mitotic Index			
Myocardial sections			
4 months	6	781[(2)]	130±31
27 months	6	794[(2)]	132±27
Isolated myocytes			
4 months	5	92140[(2)]	18428±4258
27 months	7	55490[(2)]	7927±4517
Telomere Length			
3 months	6	1404[(2)]	234±183
27 months	6	1298[(2)]	216±134
BrdU Labeling in vitro			
3 months			
Control	5	3700[(2)]	740±267
IGF-1	5	1562[(2)]	312±163
HGF	5	2273[(2)]	455±177
IGF-1 + HGF	5	1718[(2)]	344±226
AngII	5	4408[(2)]	882±211
27 months			
Control	5	4326[(2)]	865±140
IGF-1	5	2807[(2)]	561±193
HGF	5	4010[(2)]	802±247
IGF-1 + HGF	5	2831[(2)]	566±136
AngII	5	4845[(2)]	969±89

Apoptosis Labeling in vitro			
3 months			
Control	5	4790[3]	958±180
AngII	5	2162[3]	432±129
AngII + IGF-1	5	5042[3]	1008±89
AngII + HGF	5	2270[3]	454±123
AngII + IGF-1 + HGF	5	5025[3]	1005±41
27 months			
Control	5	5154[3]	1031±27
AngII	5	4812[3]	962±151
AngII + IGF-1	5	5078[3]	1016±14
AngII + HGF	5	4835[3]	967±163
AngII + IGF-1 + HGF	5	5127[3]	1025±7
ELISA of IGF-1, HGF and Ang II			
3 months	5	N/A	N/A
27 months	5	N/A	N/A
Real-Time RT-PCR			
3 months	5	N/A	N/A
12 months	6	N/A	N/A
16 months	6	N/A	N/A
24 months	5	N/A	N/A
Western Blotting			
3 months	5	N/A	N/A
27 months	5	N/A	N/A
Telomerase Activity			
3 months	5	N/A	N/A
27 months	5	N/A	N/A

8-OHdG in vitro			
3 months, SFM	5	2051[3]	410±71
3 months, AngII	5	1460[3]	292±56
27 months, SFM	5	1444[3]	289±90
27 months, AngII	5	1108[3]	222±43
Growth Factors and their Receptors			
IGF-1			
4 months	6	282[3]	47±8
12 months	6	337[3]	56±11
20 months	6	490[3]	82±10
28 months	5	370[3]	74±14
IGF-1R			
4 months	6	273[3]	46±6
12 months	6	314[3]	52±15
20 months	6	385[3]	64±20
28 months	5	384[3]	77±18
HGF			
4 months	6	294[3]	49±8
12 months	6	309[3]	52±8
20 months	6	401[3]	67±17
28 months	5	317[3]	63±17
c-Met			
4 months	6	257[3]	43±8
12 months	6	290[3]	48±16
20 months	6	383[3]	64±21
28 months	5	325[3]	65±31
AngII			
4 months	6	472[3]	79±14
12 months	6	478[3]	80±16
20 months	6	450[3]	75±16

28 months	5	371[3]	74±18
AT1R			
4 months	6	449[3]	75±13
12 months	6	464[3]	77±18
20 months	6	480[3]	80±12
28 months	5	369[3]	74±17
Growth Factor Stimulation of Migration			
4 months			
HGF	4	421[3]	105±18
IGF-1	4	343[3]	86±18
HGF + IGF-1	4	402[3]	101±15
27 months			
HGF	4	328[3]	82±18
IGF-1	4	290[3]	73±7
HGF + IGF-1	4	315[3]	79±18
BrdU Labeling in GF-treated rats			
16-17 months			
Untreated			
Myocytes	5	2639[2]	528±72
SMCs	5	1534[2]	307±56
ECs	5	1769[2]	354±117
Treated			
Myocytes	5	1967[2]	393±46
SMCs	5	1526[2]	305±42
ECs	5	1428[2]	286±75
21-22 months			
Untreated			
Myocytes	5	1975[2]	395±80
SMCs	5	1308[2]	262±40

ECs	5	1429[(2)]	286±54
Treated			
Myocytes	5	1251[(2)]	250±43
SMCs	5	1441[(2)]	288±66
ECs	5	1580[(2)]	316±57
28-29 months			
Untreated			
Myocytes	6	2293[(2)]	382±37
SMCs	6	1601[(2)]	267±40
ECs	6	1940[(2)]	323±83
Treated			
Myocytes	6	1042[(2)]	174±37
SMCs	6	1754[(2)]	292±27
ECs	6	1667[(2)]	278±25
$p16^{INK4a}$ Labeling in GF-treated Rats			
Untreated	8	1726[(2)]	216±15
Treated	12	3115[(2)]	260±25
Anatomy			
15 months	6	N/A	N/A
16-17 months untreated	10	N/A	N/A
16-17 months treated	9	N/A	N/A
20 months	9	N/A	N/A
21-22 months untreated	10	N/A	N/A
21-22 months treated	9	N/A	N/A
27 months	8	N/A	N/A
28-29 months untreated	10	N/A	N/A
28-29 months treated	18	N/A	N/A
Hemodynamics			

15 months	9	N/A	N/A
16-17 months untreated	10	N/A	N/A
16-17 months treated	6	N/A	N/A
20 months	8	N/A	N/A
21-22 months untreated	10	N/A	N/A
21-22 months treated	9	N/A	N/A
27 months	7	N/A	N/A
28-29 months untreated	10	N/A	N/A
28-29 months treated	12	N/A	N/A
Echocardiography			
Untreated	9	N/A	N/A
Treated	14	N/A	N/A
Mortality			
Untreated	32	N/A	N/A
Treated	48	N/A	N/A

(1) Area of tissue sampled, mm^2; (2) Number of nuclei analyzed; (3) Number of counted cells; N/A, not applicable.

Supplemental Table II: Antibodies and their labeling

Protein	Antibody	Labeling	Fluorochrome(s)
Stem cell markers			
c-kit	goat polyclonal	direct and indirect	F, T, Cy5, QD655
MDR-1	mouse monoclonal	direct and indirect	F, T, Cy5, QD655
Sca-1	rat monoclonal	direct and indirect	F, T, Cy5, QD655
Structural proteins of myocardial cells			
α-sarcomeric actin	mouse monoclonal	direct and indirect	F, T, Cy5, QD655
β-myosin heavy chain	mouse monoclonal	direct and indirect	T, QD655
von Willebrand factor	sheep polyclonal	direct and indirect	T, Cy5, QD655
α-smooth muscle actin	mouse monoclonal	direct and indirect	F, T, Cy5, QD655
Transcription factors of myocardial cells			
MEF2C	goat polyclonal	direct and indirect	T, Cy5, QD655
GATA-4	mouse monoclonal	direct and indirect	T, Cy5, QD655
Nkx2.5	goat polyclonal	direct and indirect	T, Cy5, QD655
Growth factors			
HGF	rabbit polyclonal	direct and indirect	T, Cy5, QD605
IGF-1	goat polyclonal	direct and indirect	T, Cy5, QD605
AngII	rabbit polyclonal	direct and indirect	T, Cy5, QD605
c-Met	rabbit polyclonal	direct and indirect	T, Cy5, QD605
IGF-1R	mouse monoclonal	direct and indirect	T, Cy5, QD605
AT1 receptor	rabbit polyclonal	direct and indirect	T, Cy5, QD605
Other stainings			
Ki67	rabbit polyclonal	direct and indirect	Cy5, QD655
BrdU	mouse monoclonal	direct and indirect	Cy5, QD655
Phospho-H3	rabbit polyclonal	direct and indirect	Cy5, QD655
$p16^{INK4a}$	mouse monoclonal	direct and indirect	Cy5, QD655
8-OH-dG	rabbit polyclonal	direct and indirect	Cy5, QD655

EGFP	rabbit polyclonal	direct and indirect	Cy5, QD655
Telomeres		direct	F
TUNEL	TdT/dUTP	direct	F
Laminin	rabbit polyclonal	direct and indirect	Cy5, QD655

Direct labeling: Primary antibody conjugated with the fluorochrome. Indirect labeling: species-specific secondary antibody conjugated with the fluorochrome. F: fluorescein isothiocyanate, T: tetramethyl rhodamine isothiocyanate, Cy5: cyanine 5, QD655: quantum dots with emission at 655 nm, QD605: quantum dots with emission at 605 nm.

Supplemental TABLE III: Primers and annealing temperatures used in the real-time RT-PCR

Gene	Forward primer (5'→ 3')	Reverse primer (5'→ 3')	Annealing T (ºC)
IGF-1 (Igf1)	CGAACCTCCAATAAAGATACAC	CAACACTCATCCACAATGCC	61
IGF-1R (Igf1r	CGAGCAAGTTCTTCGTTTCGT	TGTACTGCCAGCACATGCG	61
HGF (Hgf)	TGCCCTATTTCCCGTTGTG	AATGCCATTTACAACTCGCAGTT	61
c-Met (Met)	ACAACAAAACGGGTGCGAAA	TCATGAGCTCCCAGAGAAGCA	61
Renin (Ren1)	CCTGGGAGTCAAAGAGAAGAG	GTATAGAACTTGCGGATGAAGG	62
Aogen (Agt)	ATCAACAGGTTTGTGCAGGC	GTTGTCCACCCAGAACTCATGG	66
AT1 receptor (Agtr1)	GTCCTCTCAGCTCTGCCACATT	CACTTGACCTTTACCTGGTGATCA	64
B-actin (Actb)	ACCCTGTGCTGCTCACCGAG	CCAGTGGTACGACCAGAGGC	Same as target gene

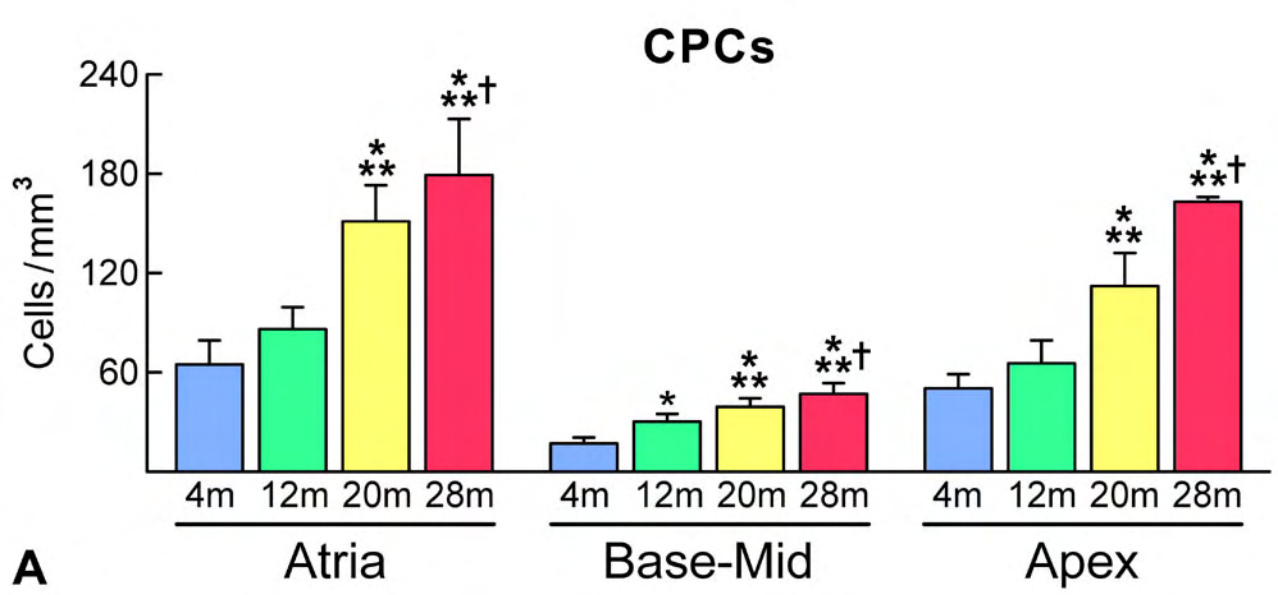
CPCs
240
180
120
60
Cells/mm3
*
**
*
**†
*
**
*
**
*
**†
*
**
*
**
*
**†
4m 12m 20m 28m
4m 12m 20m 28m
4m 12m 20m 28m
Atria
Base-Mid
Apex
A

Figure I A

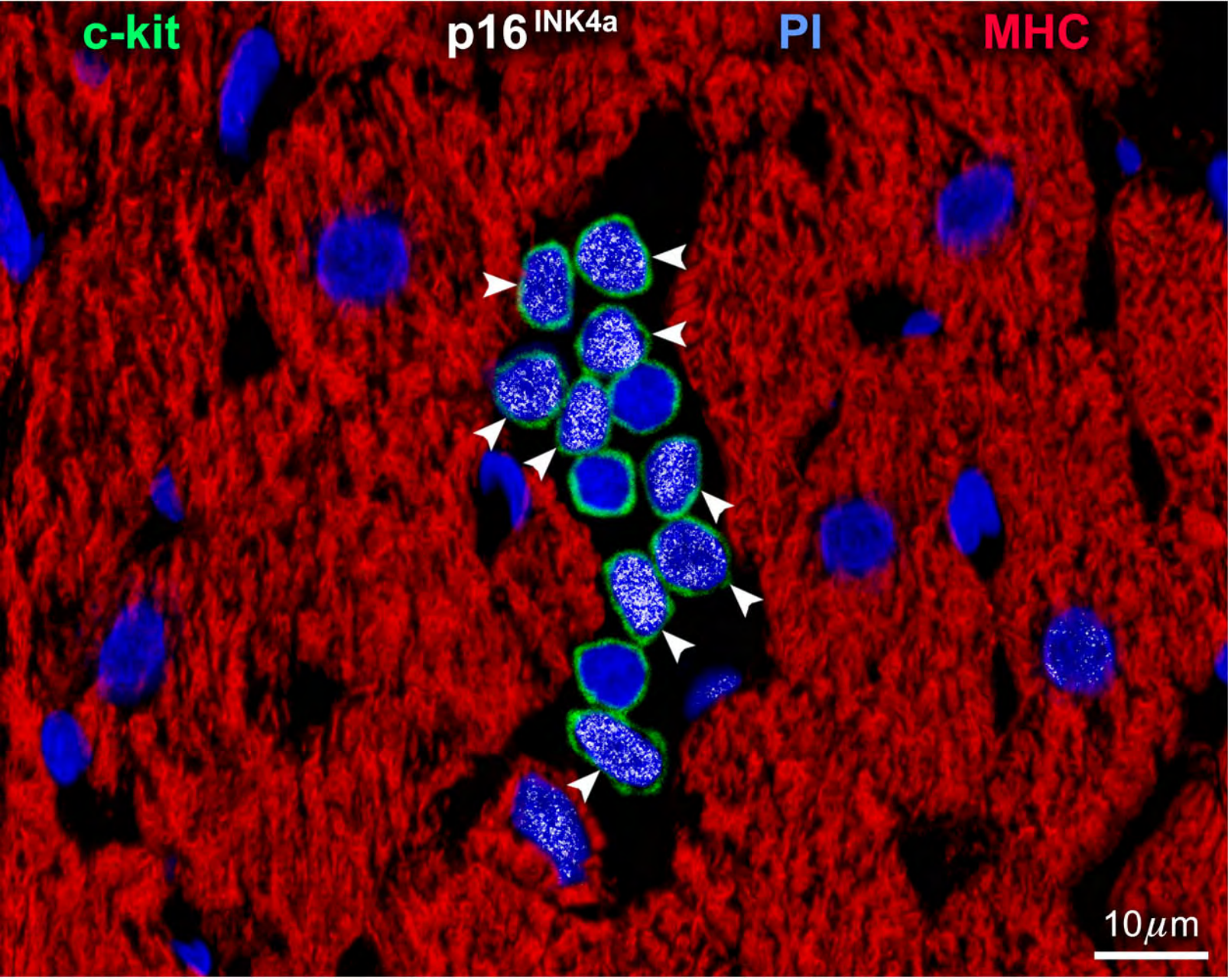
c-kit
p16 INK4a
PI
MHC
10μm

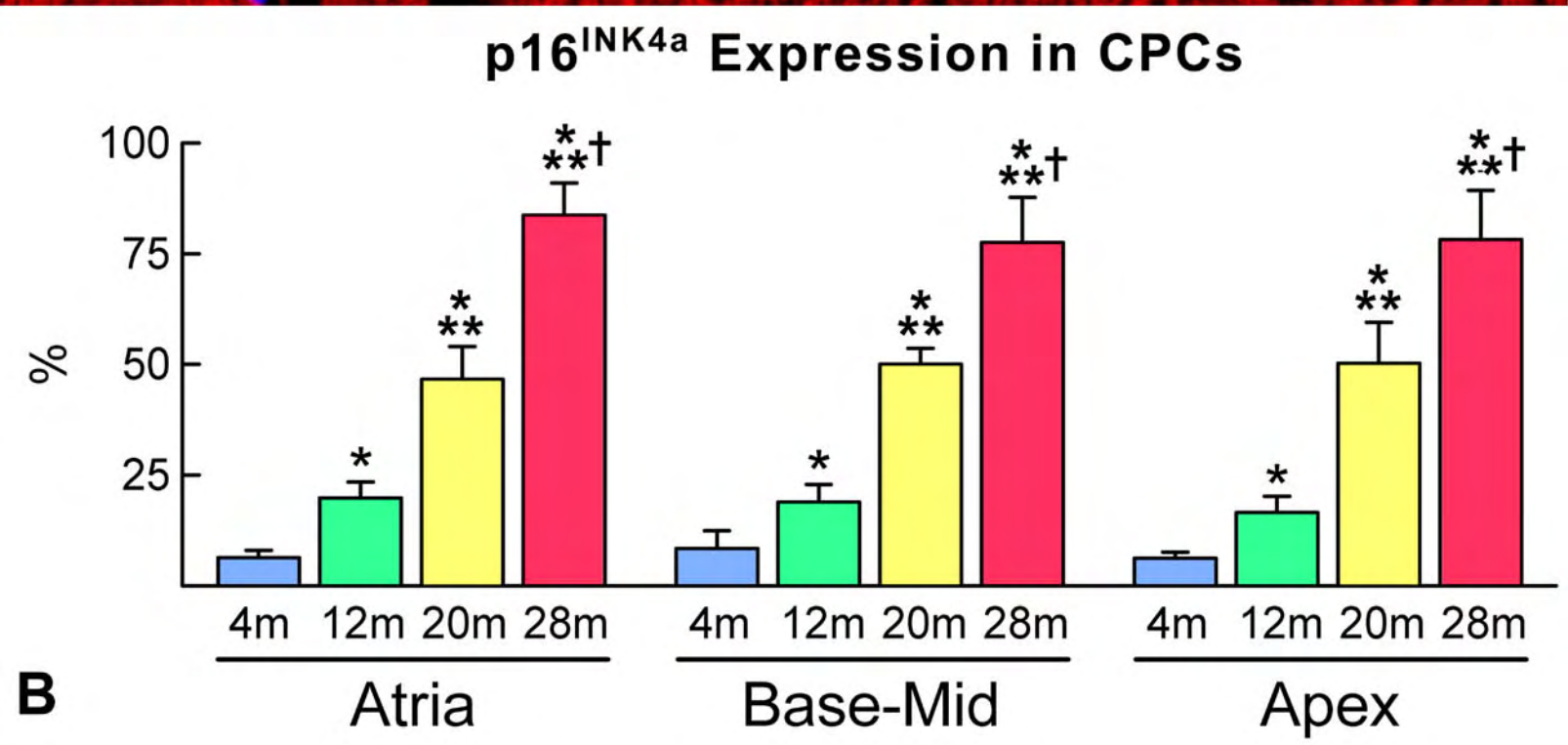
p16INK4a Expression in CPCs
100
75
50
25
%
4m
12m
20m
28m
Atria
Base-Mid
Apex
B

Figure I B

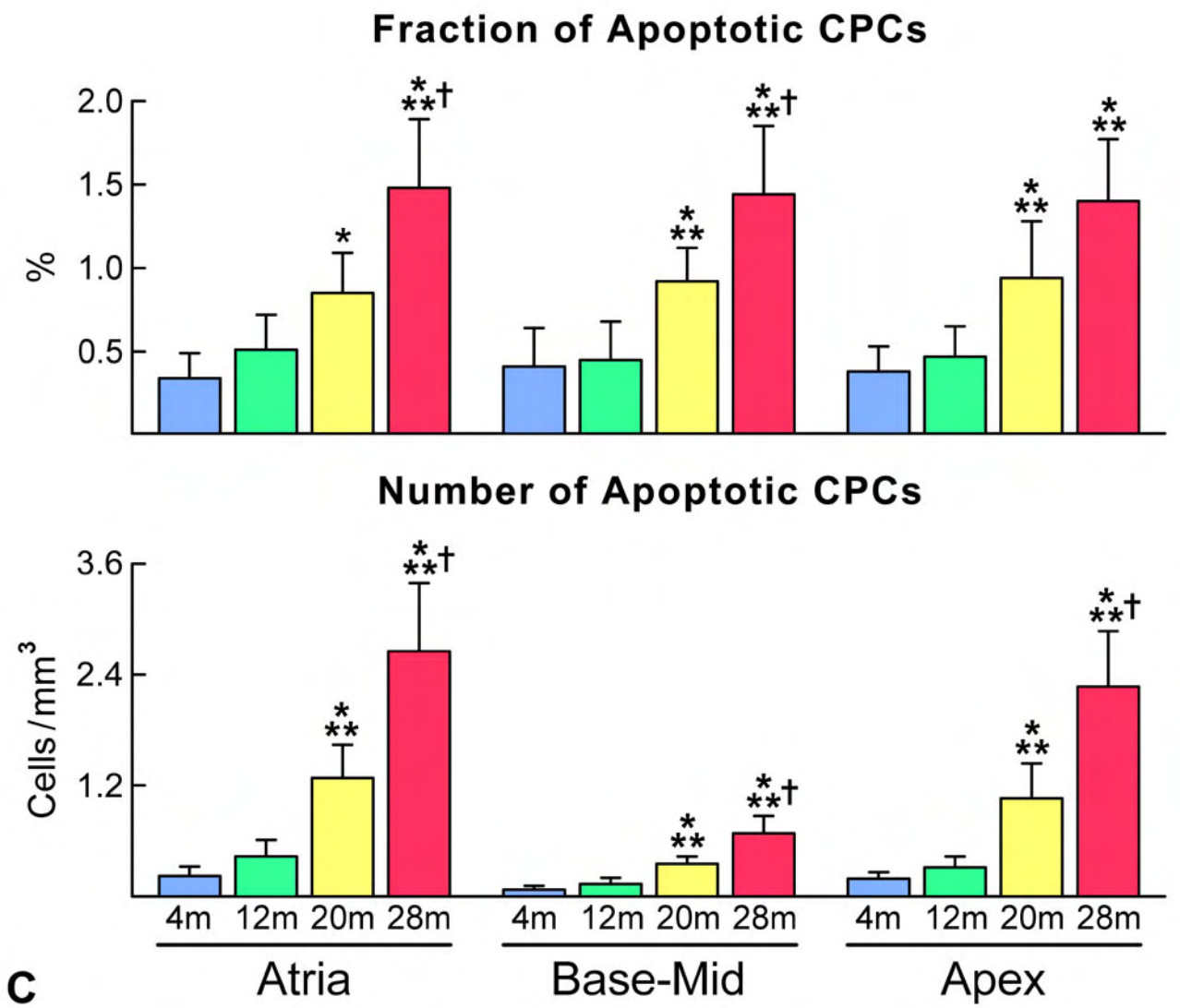
Fraction of Apoptotic CPCs
2.0
1.5
1.0
0.5
%
Number of Apoptotic CPCs
3.6
2.4
1.2
Cells / mm3
4m 12m 20m 28m
4m 12m 20m 28m
4m 12m 20m 28m
Atria
Base-Mid
Apex
C

Figure I C

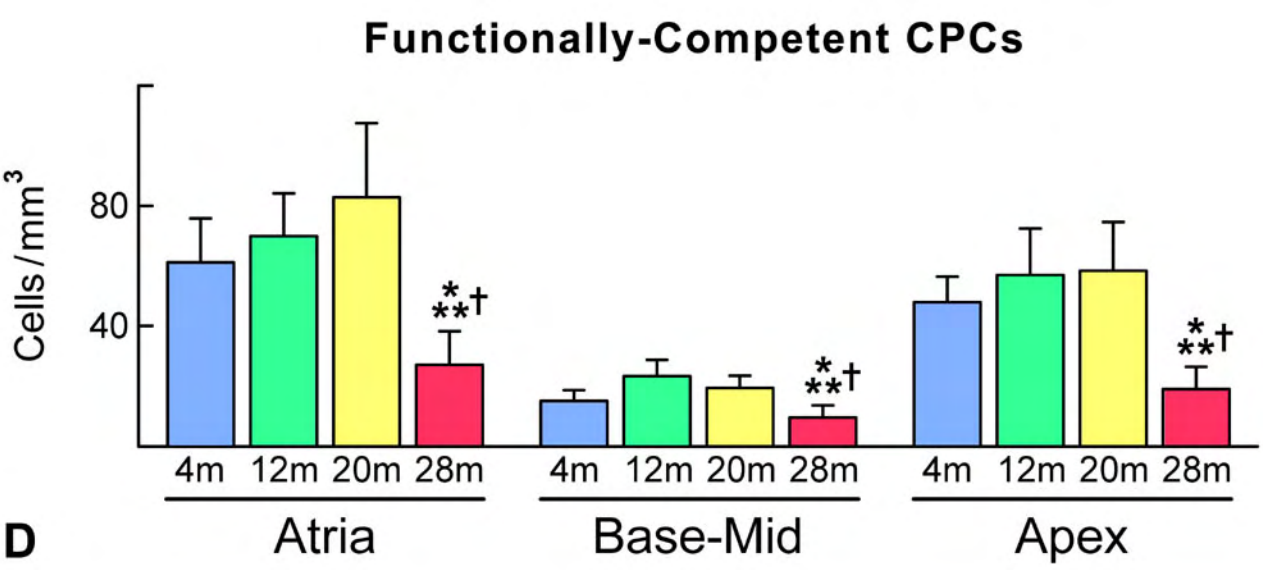
Functionally-Competent CPCs
Cells/mm3
80
40
*
**†
4m 12m 20m 28m
Atria
Base-Mid
Apex
D

Figure I D

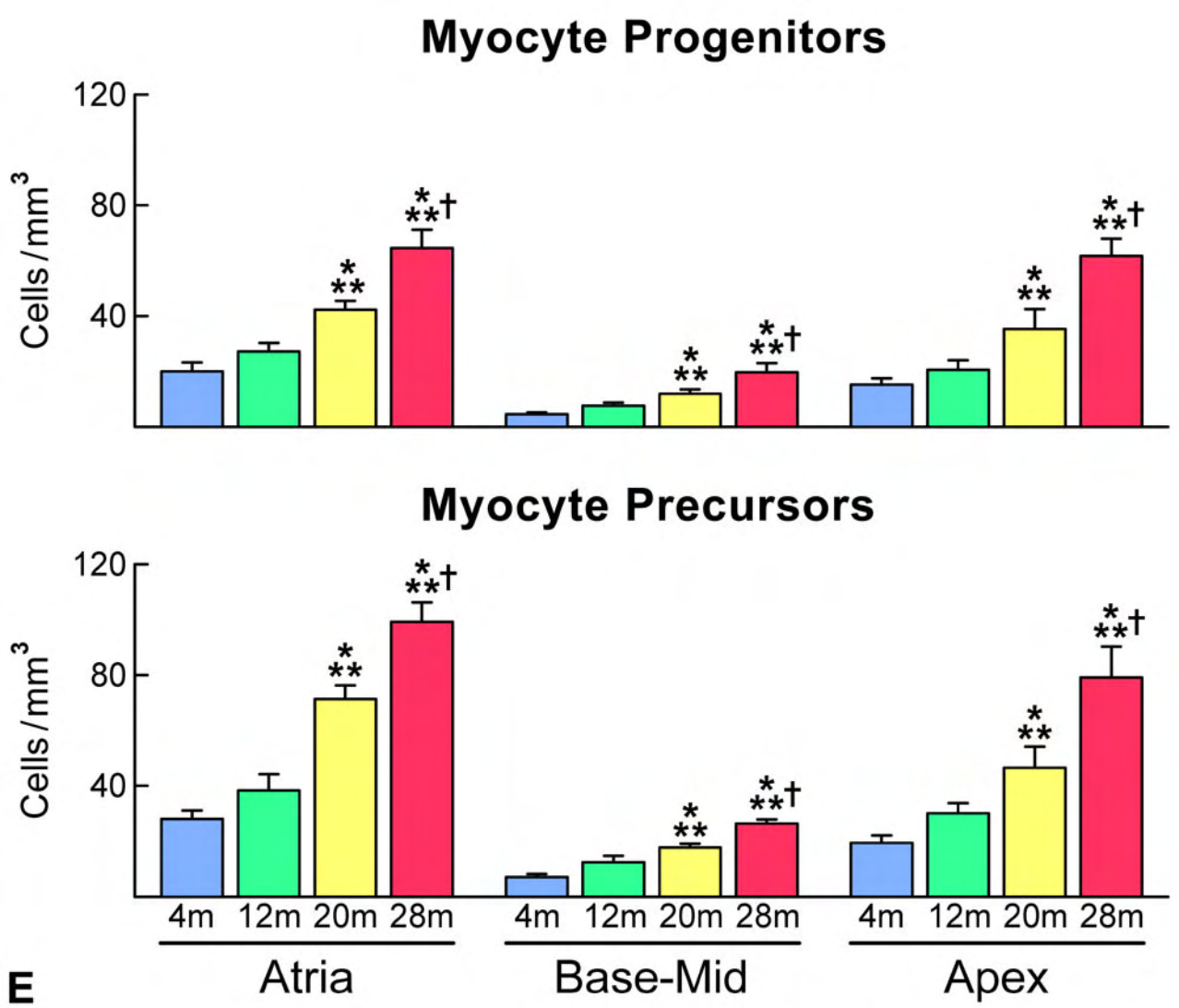
Myocyte Progenitors
120
80
40
Cells/mm3
*
**
*
**†
Myocyte Precursors
120
80
40
Cells/mm3
4m 12m 20m 28m
4m 12m 20m 28m
4m 12m 20m 28m
Atria
Base-Mid
Apex

E

Figure I E

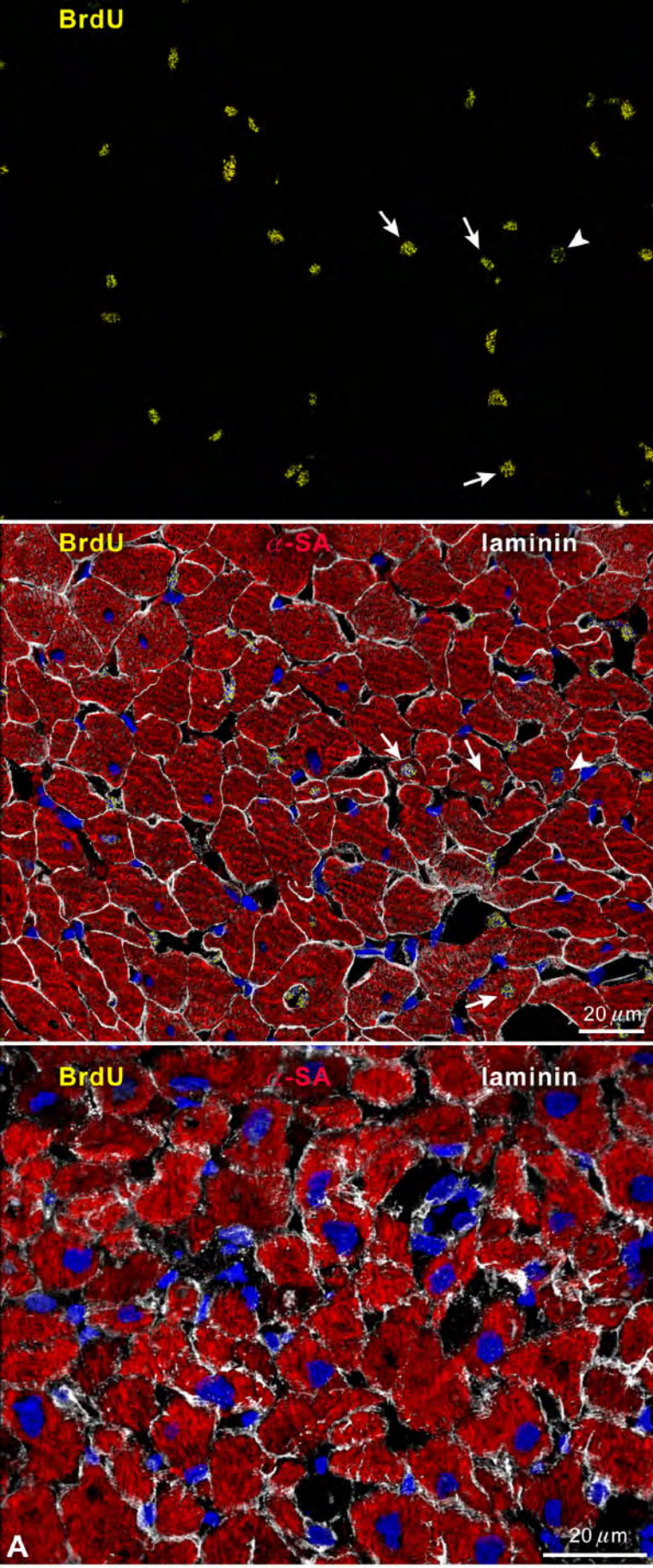

Figure II A

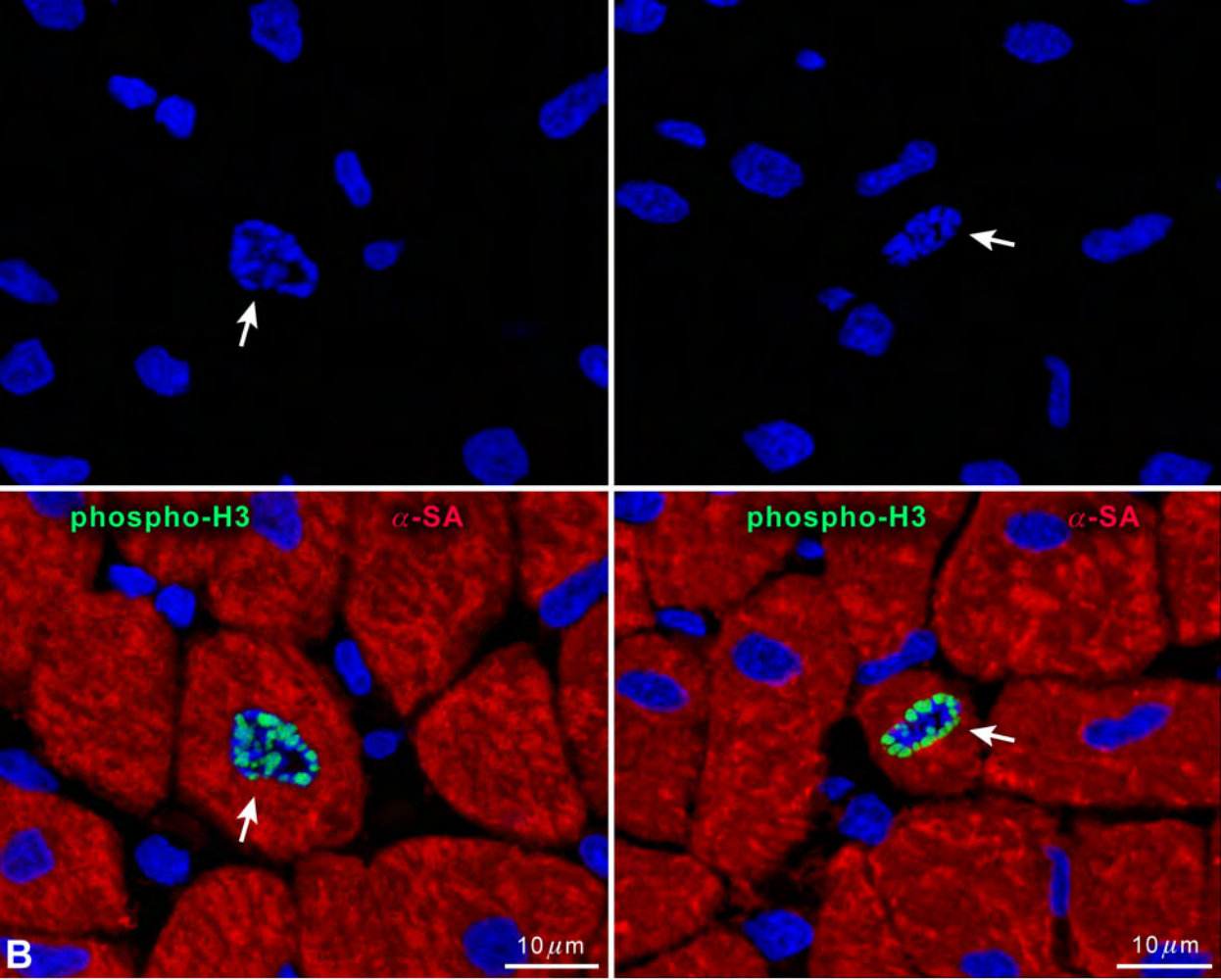

Figure II B

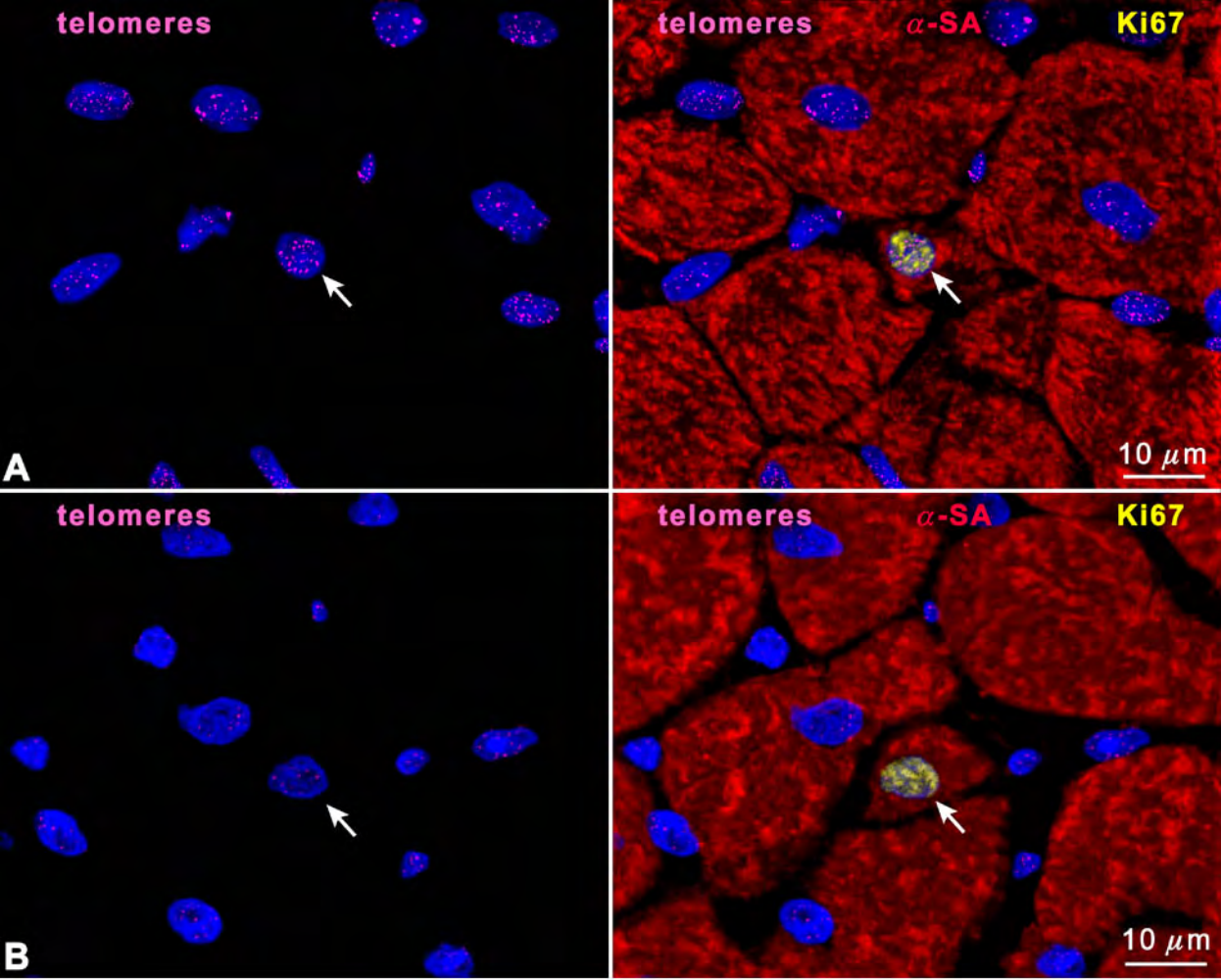
telomeres
telomeres
α-SA
Ki67
A
10 μm
telomeres
telomeres
α-SA
Ki67
B
10 μm

Figure III

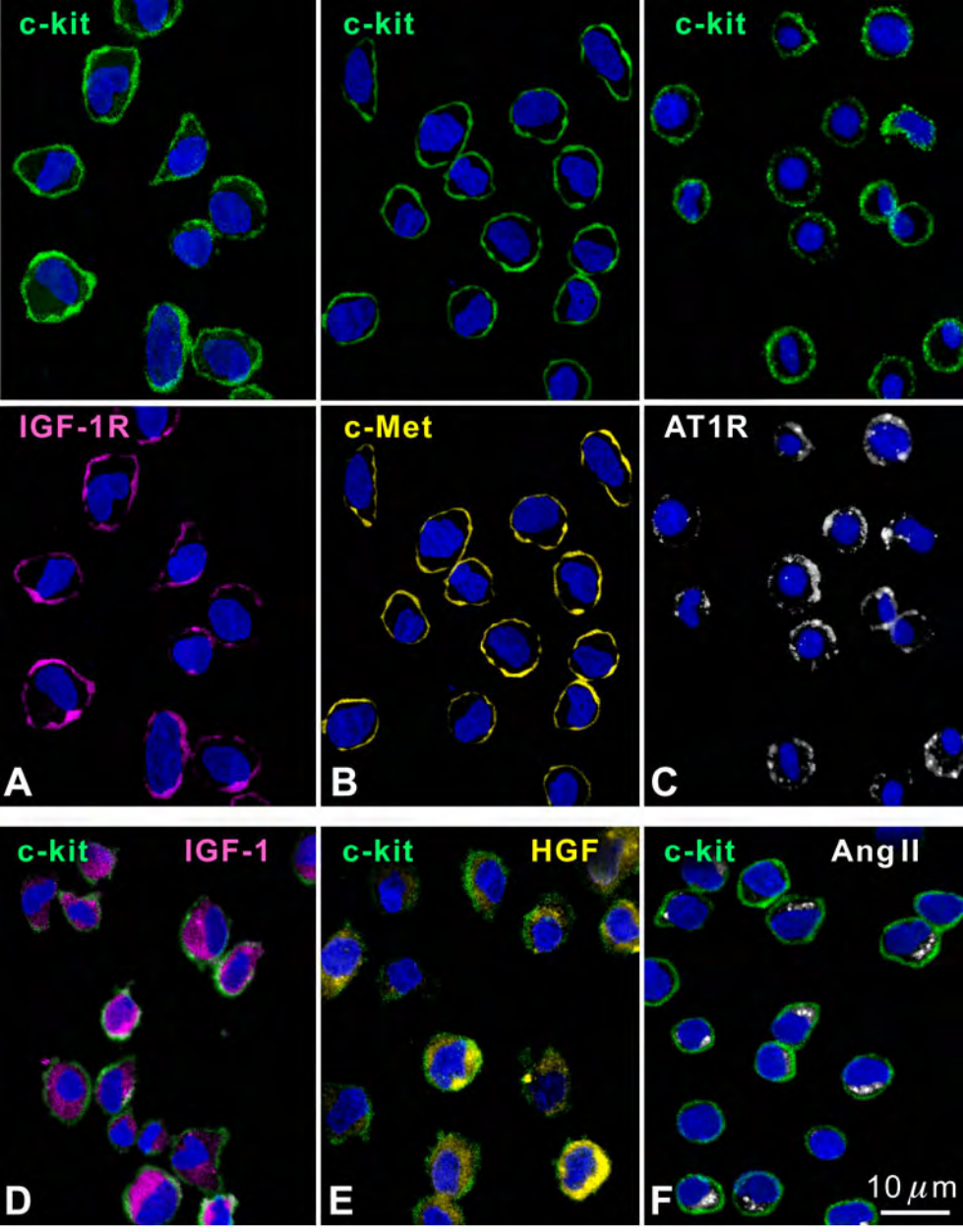
c-kit
c-kit
c-kit
IGF-1R
c-Met
AT1R
A
B
C
c-kit
IGF-1
c-kit
HGF
c-kit
Ang II
D
E
F
10 μm

Figure IV

Renin

sense

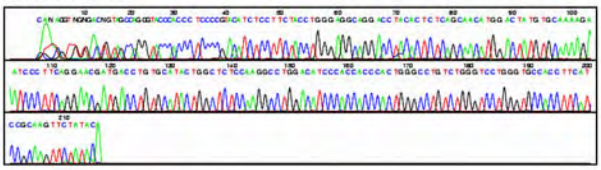

antisense

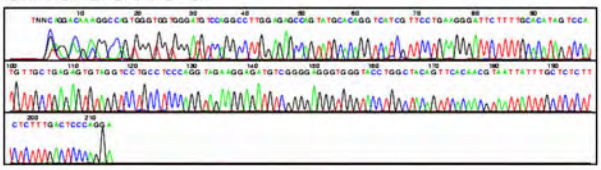

Aogen

sense

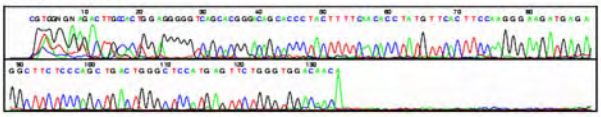

antisense

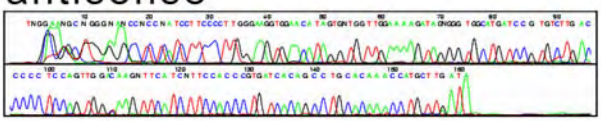

AT1

sense

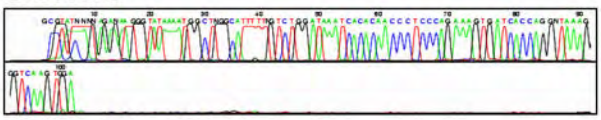

antisense

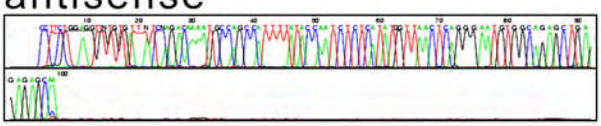

β-actin

sense

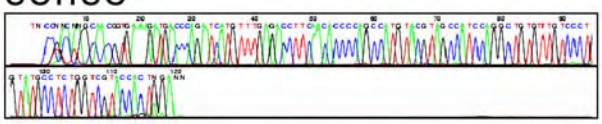

antisense

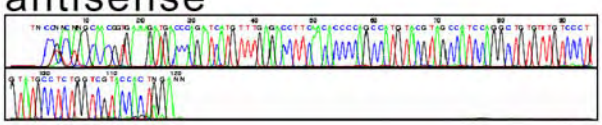

IGF-1R

sense

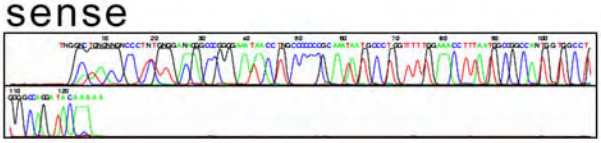

antisense

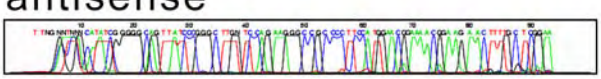

IGF-1

sense

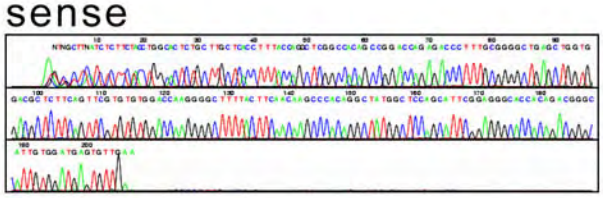

antisense

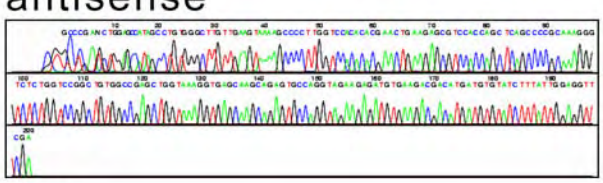

c-Met

sense

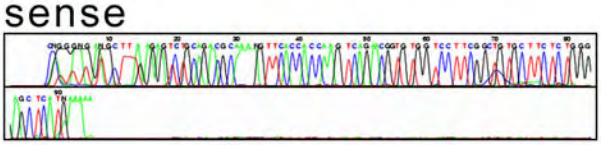

antisense

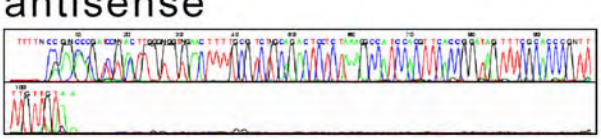

HGF

sense

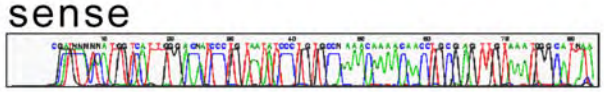

antisense

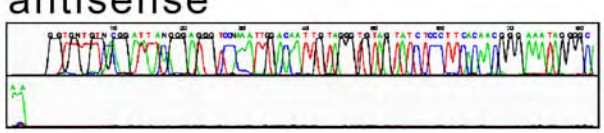

Figure V

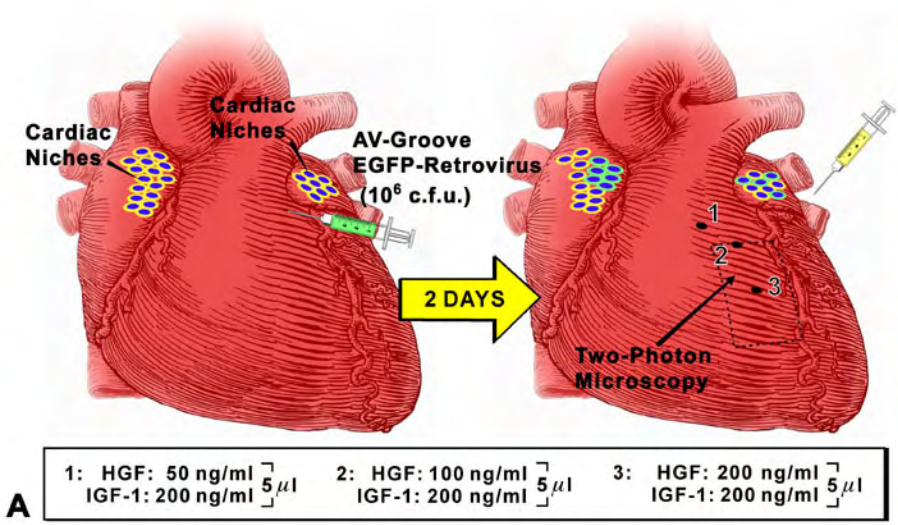
Cardiac Niches
Cardiac Niches
AV-Groove EGFP-Retrovirus (10^6 c.f.u.)
2 DAYS
1
2
3
Two-Photon Microscopy
1: HGF: 50 ng/ml
IGF-1: 200 ng/ml
5 µl
2: HGF: 100 ng/ml
IGF-1: 200 ng/ml
5 µl
3: HGF: 200 ng/ml
IGF-1: 200 ng/ml
5 µl
A

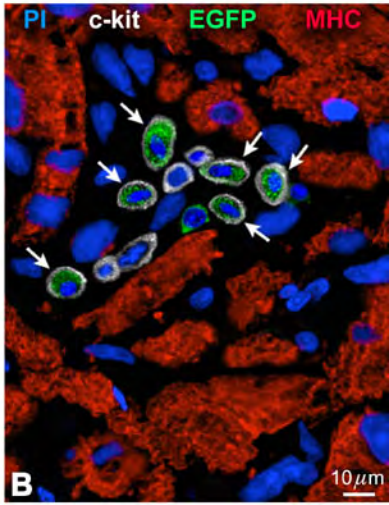
PI
c-kit
EGFP
MHC
B
10 µm

Figure VI

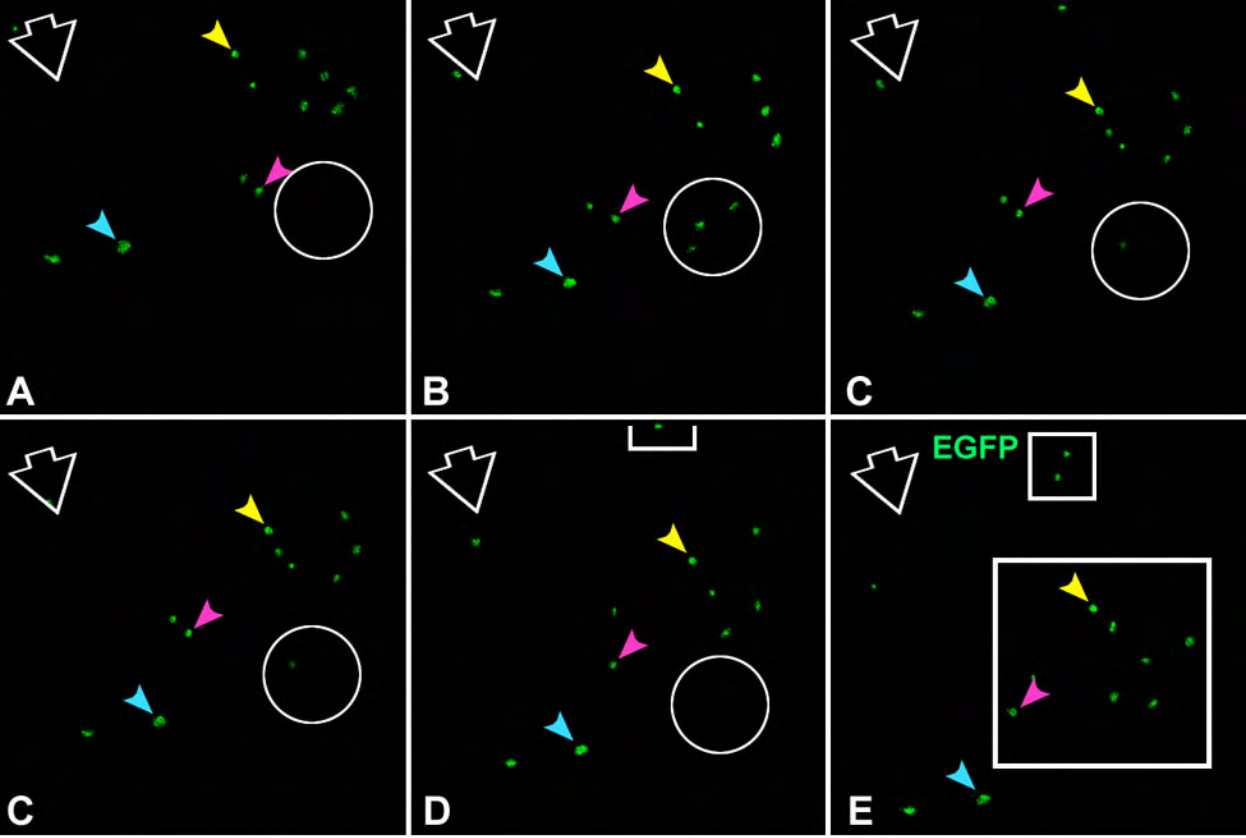

Figure VII

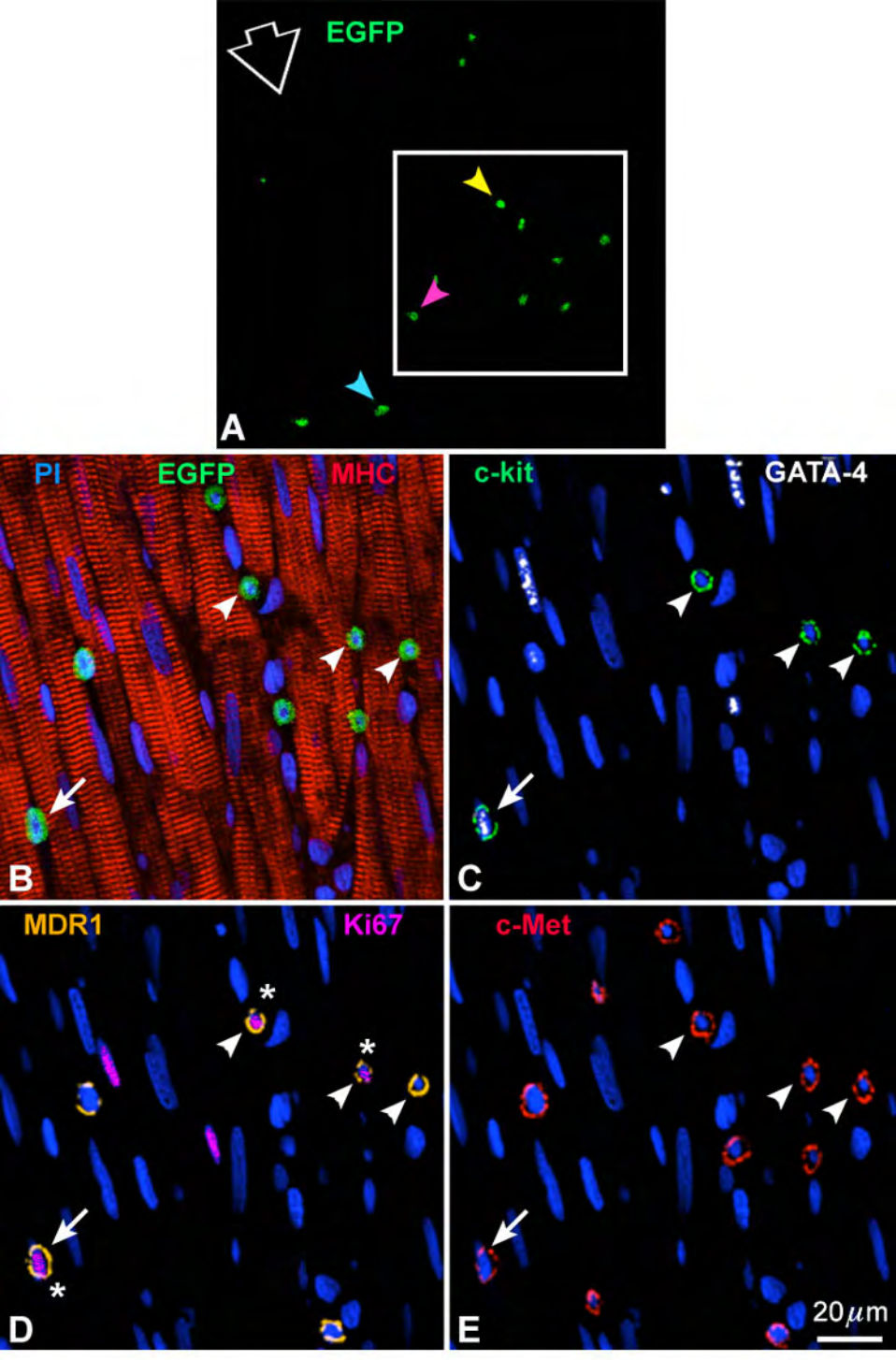

Figure VIII

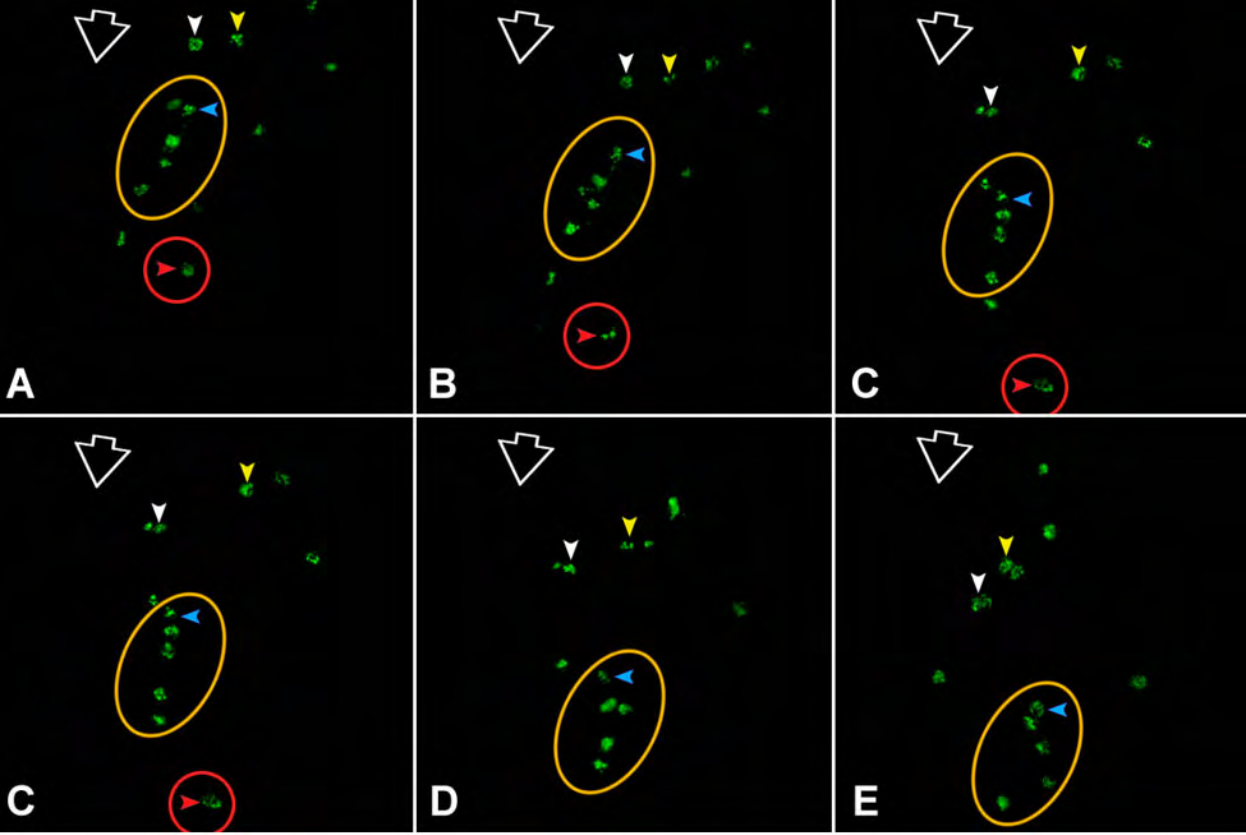

Figure IX

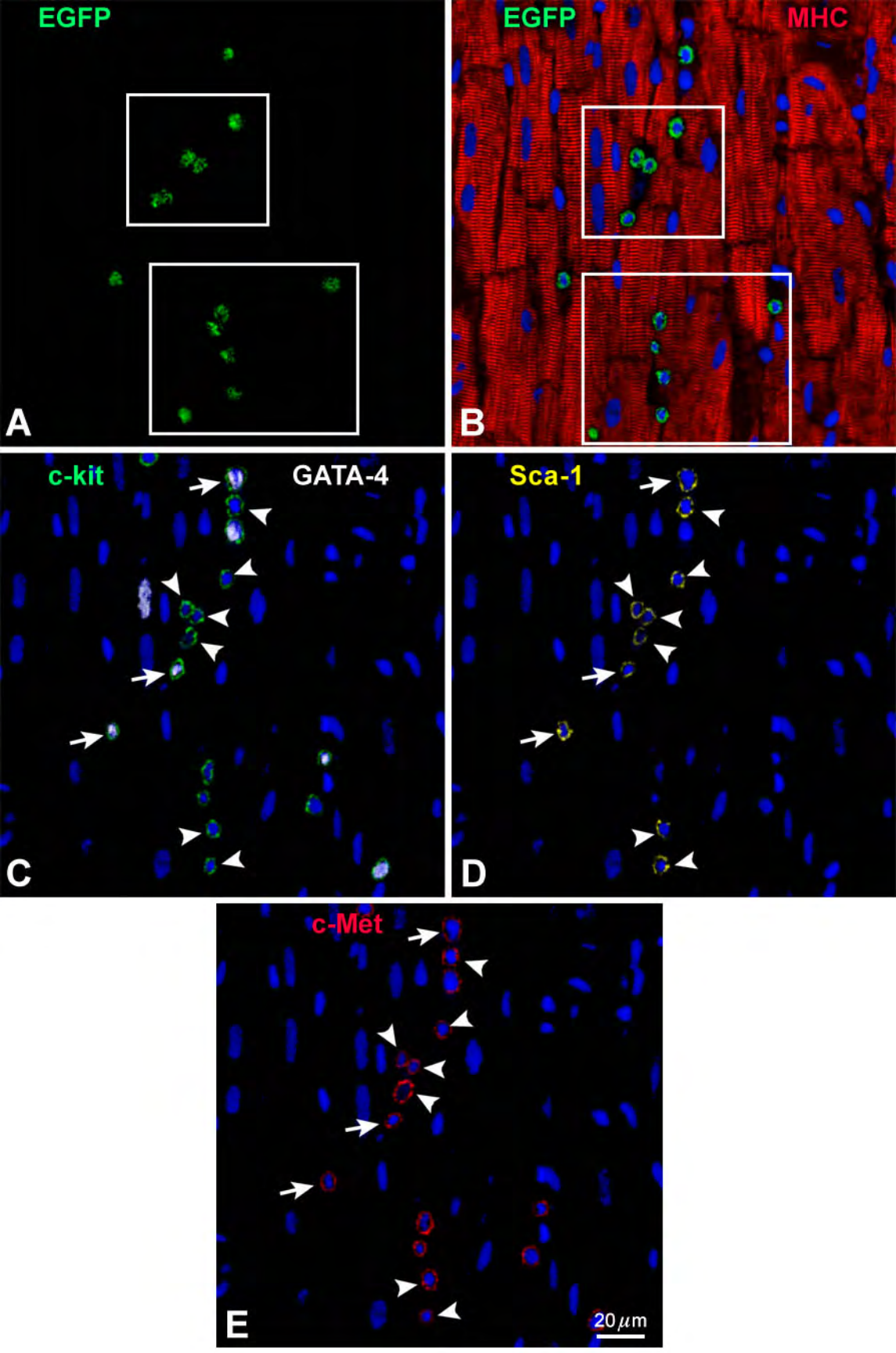

Figure X

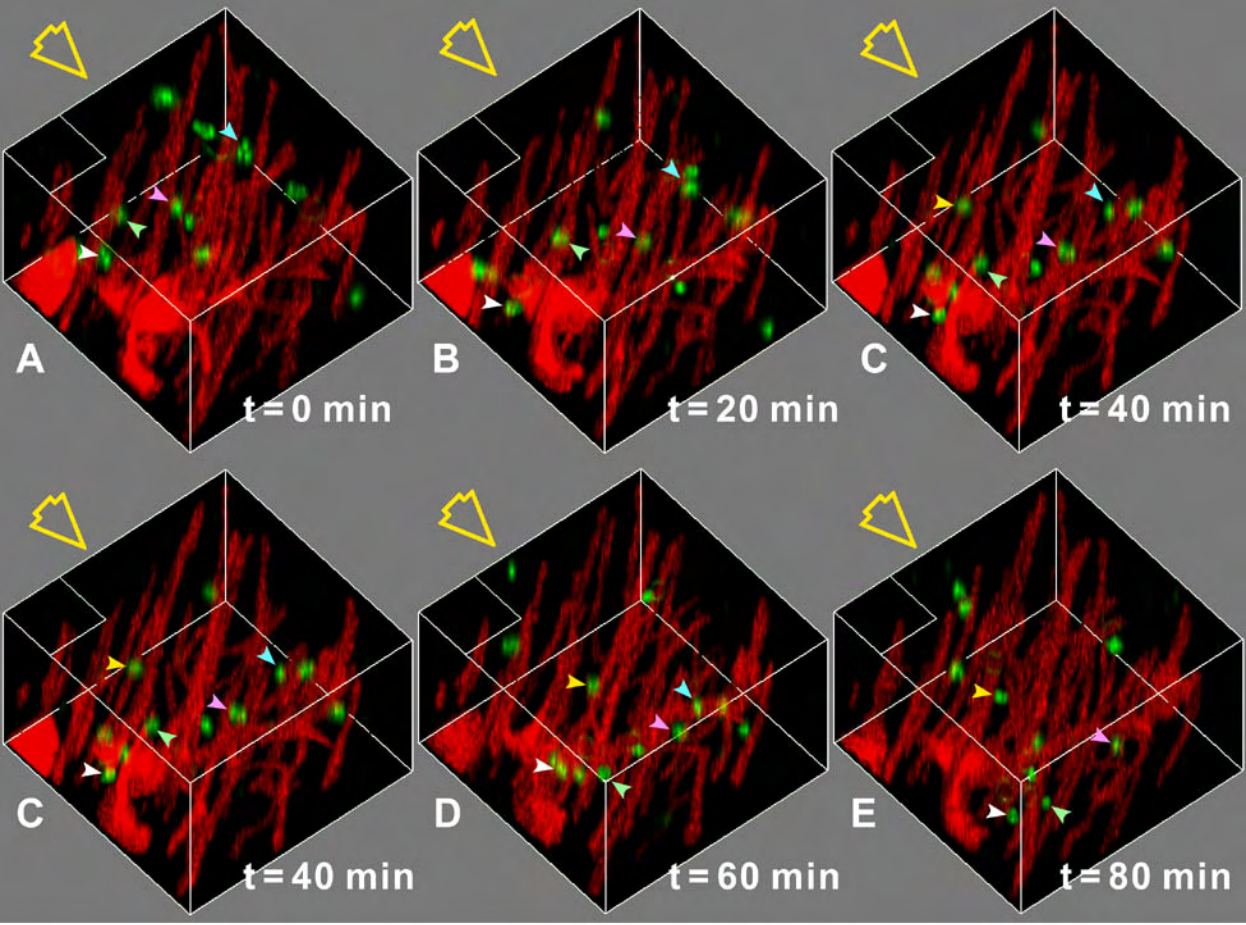

Figure XI A-E

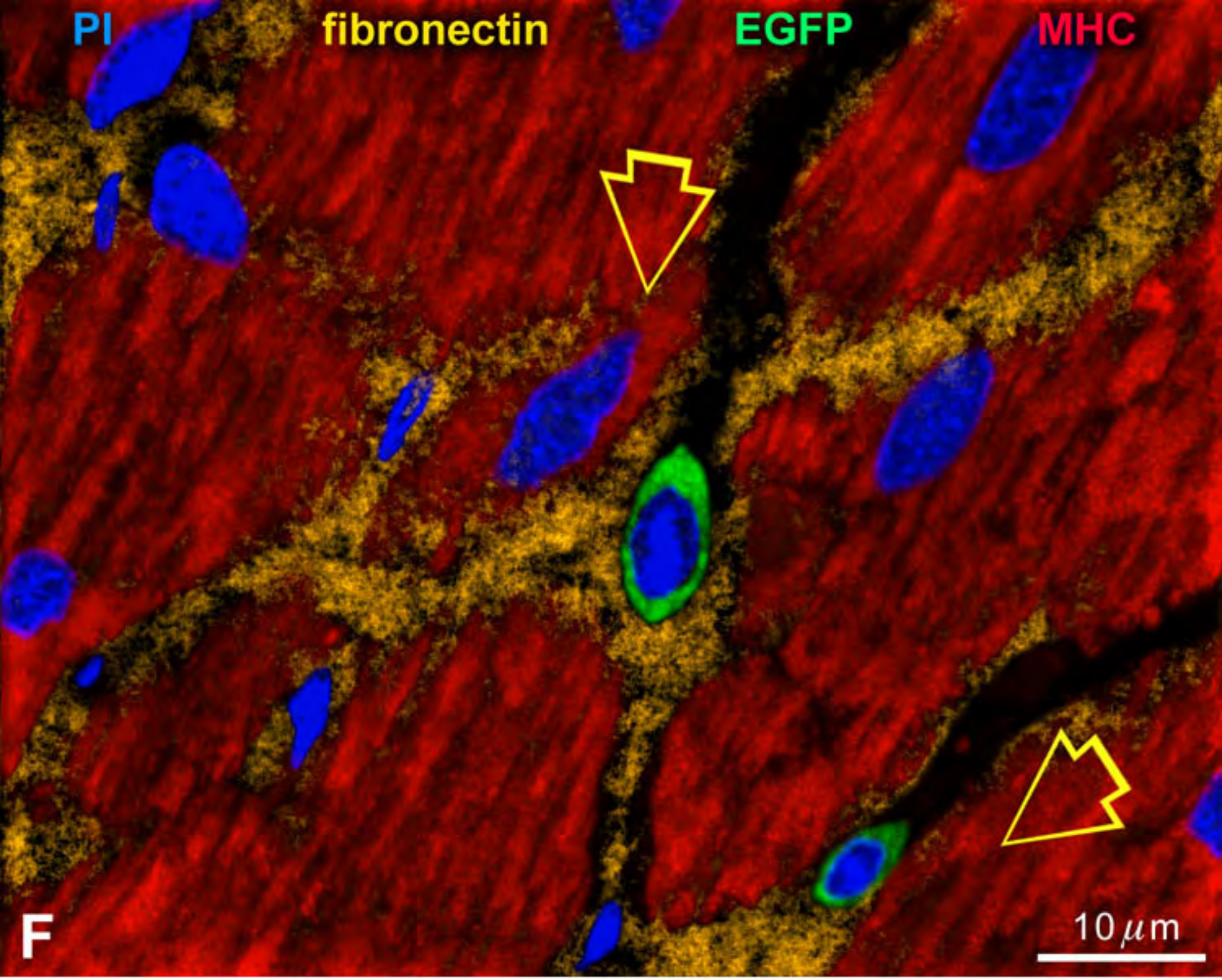

Figure XI F

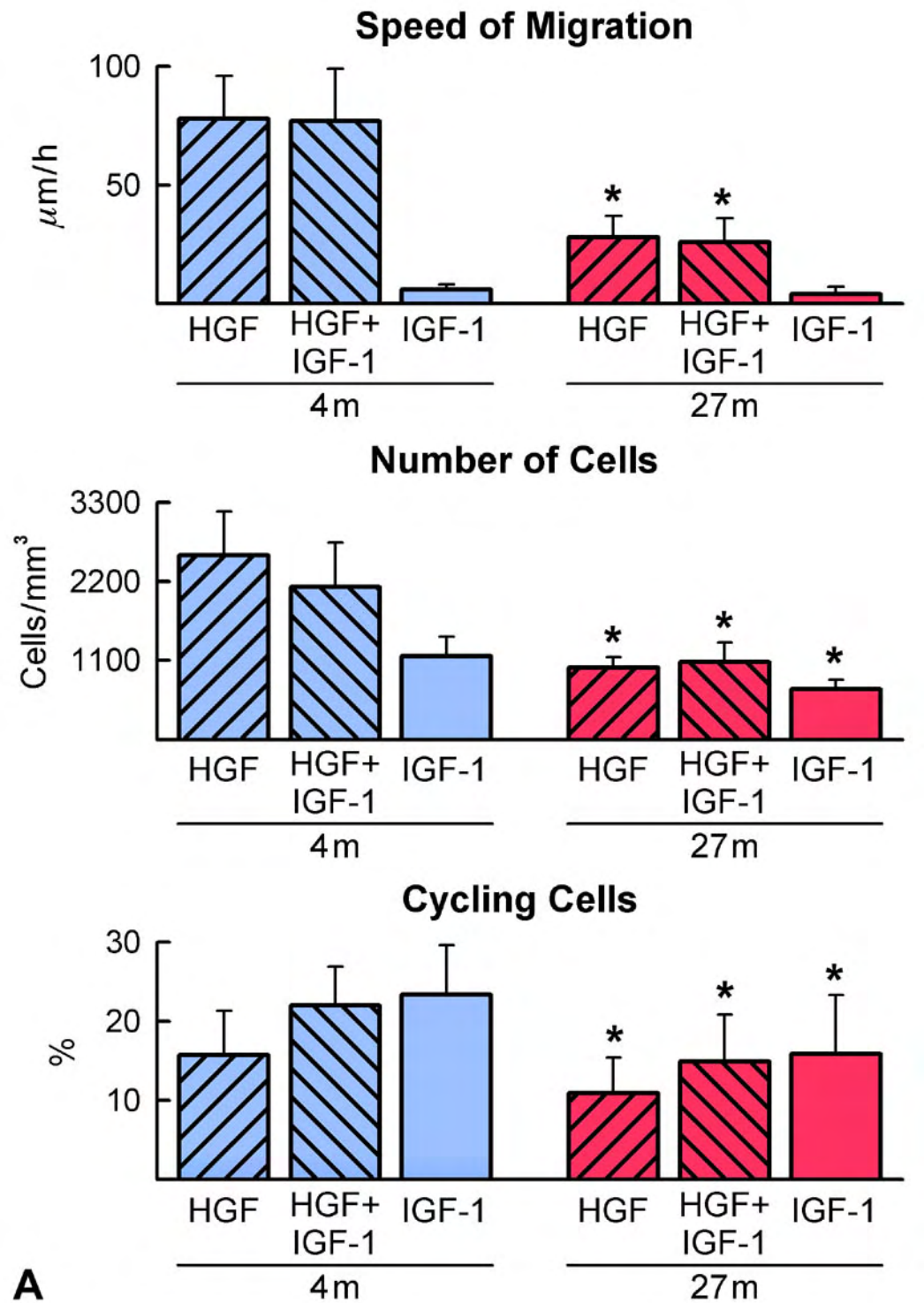
Speed of Migration
100
50
µm/h
*
*
HGF
HGF+ IGF-1
IGF-1
HGF
HGF+ IGF-1
IGF-1
4m
27m
Number of Cells
3300
2200
1100
Cells/mm3
*
*
*
HGF
HGF+ IGF-1
IGF-1
HGF
HGF+ IGF-1
IGF-1
4m
27m
Cycling Cells
30
20
10
%
*
*
*
HGF
HGF+ IGF-1
IGF-1
HGF
HGF+ IGF-1
IGF-1
4m
27m
A

Figure XII A

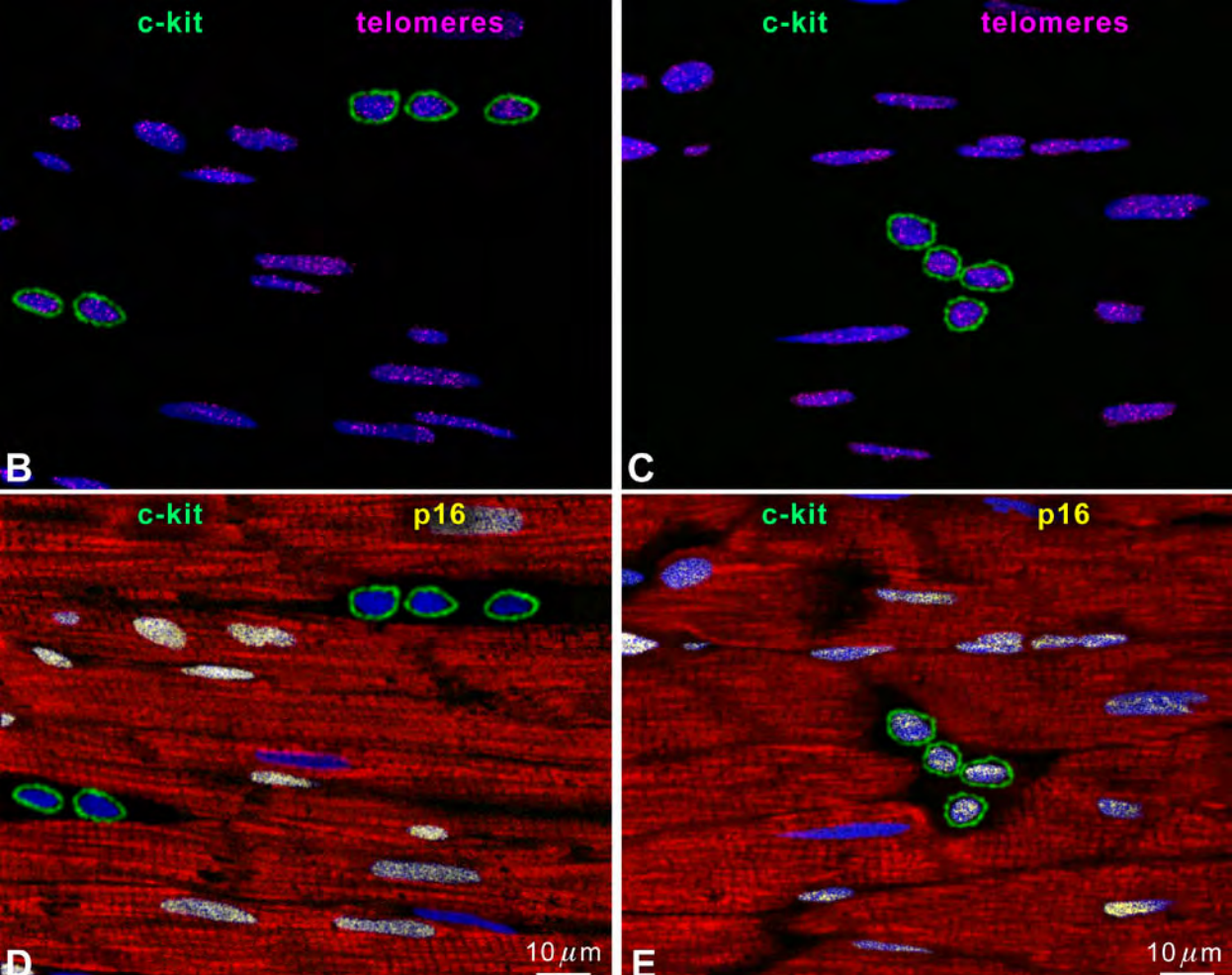

Figure XII B-E

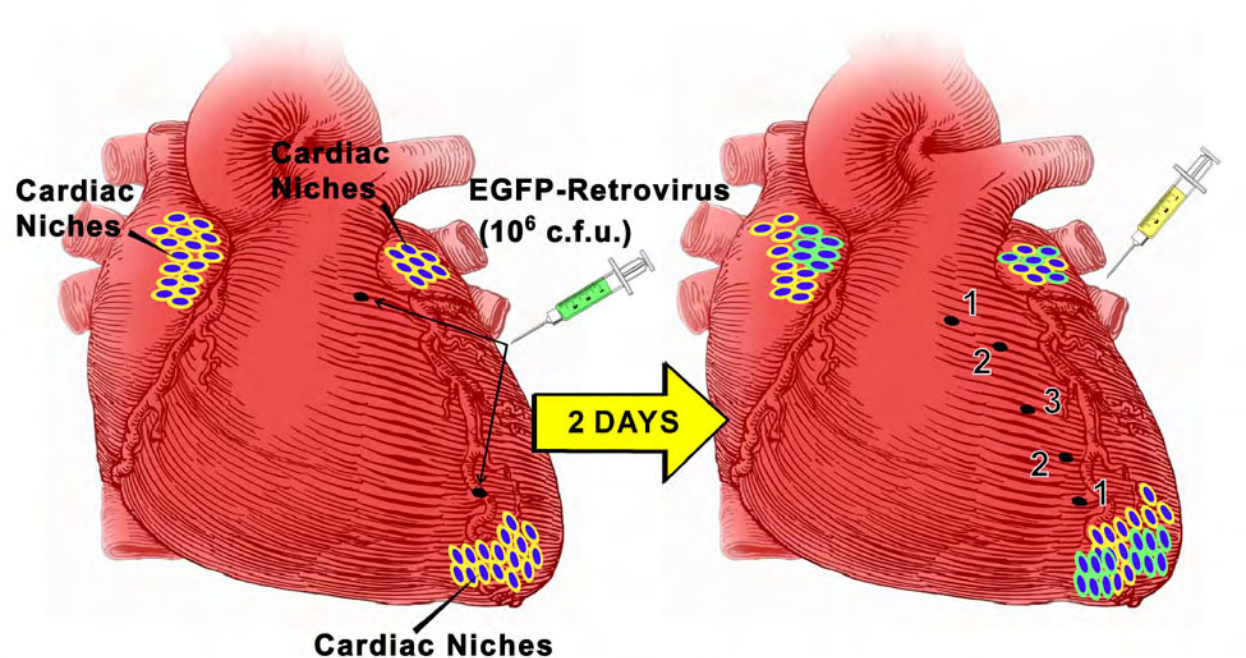

1: HGF: 50 ng/ml, IGF-1: 200 ng/ml (5 µl)	2: HGF: 100 ng/ml, IGF-1: 200 ng/ml (5 µl)	3: HGF: 200 ng/ml, IGF-1: 200 ng/ml (5 µl)

Figure XIII

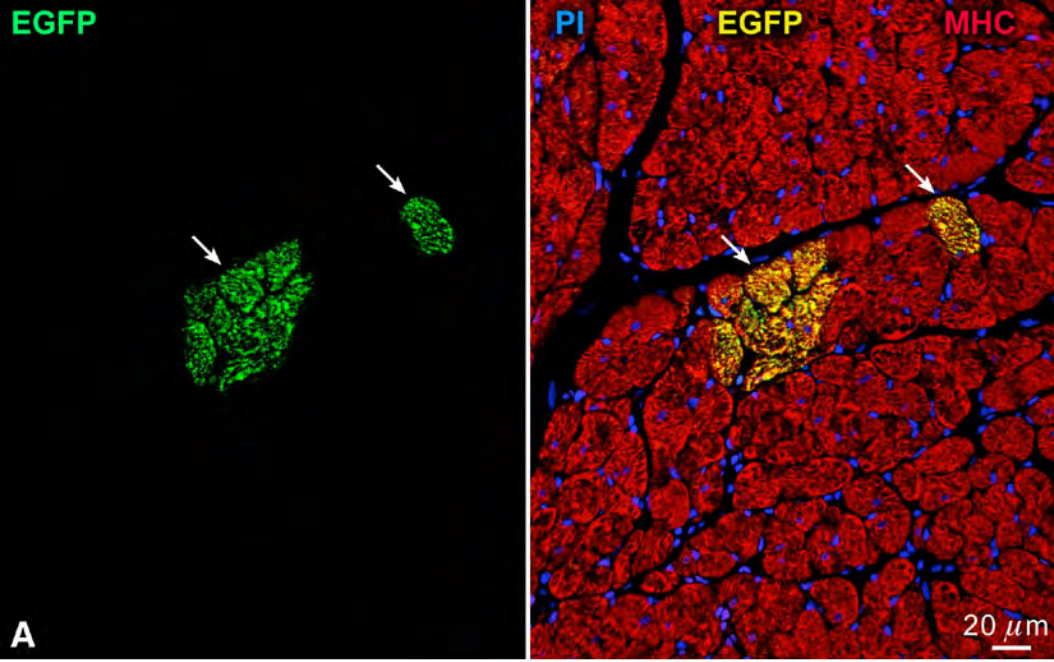

Figure XIV A

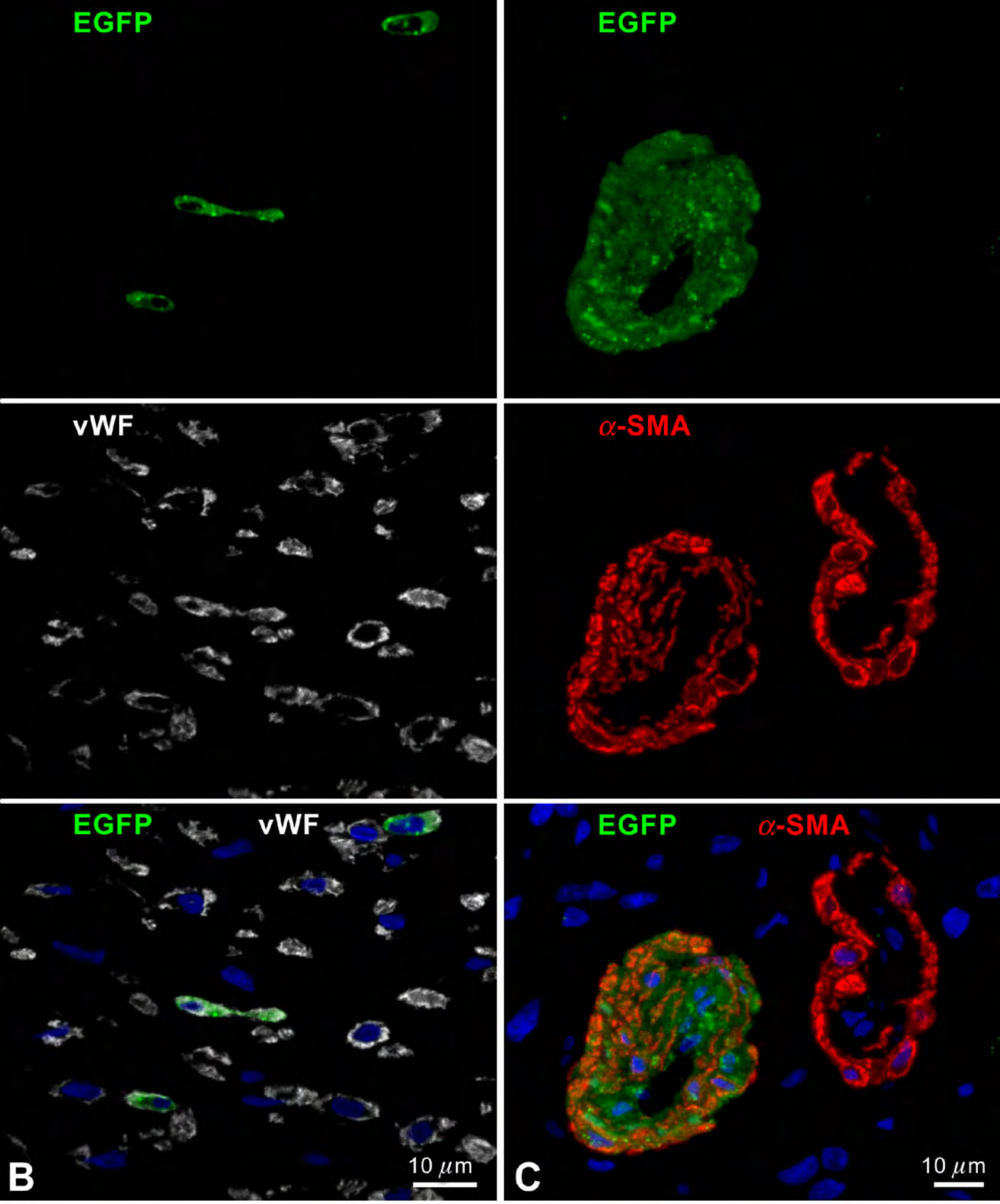

Figure XIV B, C

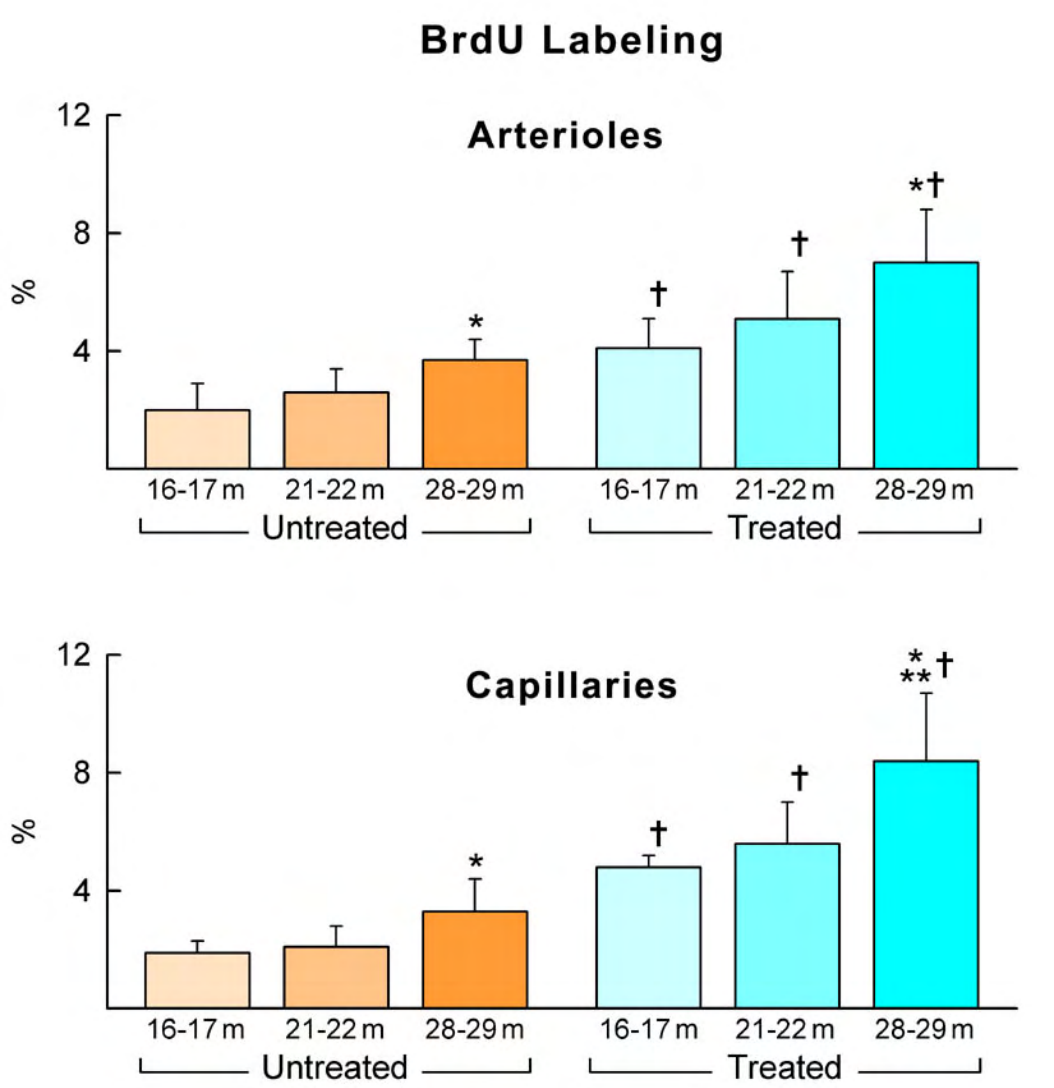
BrdU Labeling
Arterioles
12
8
4
%
*
†
†
*†
16-17 m
21-22 m
28-29 m
16-17 m
21-22 m
28-29 m
Untreated
Treated
Capillaries
12
8
4
%
*
†
†
*
**†
16-17 m
21-22 m
28-29 m
16-17 m
21-22 m
28-29 m
Untreated
Treated

Figure XV

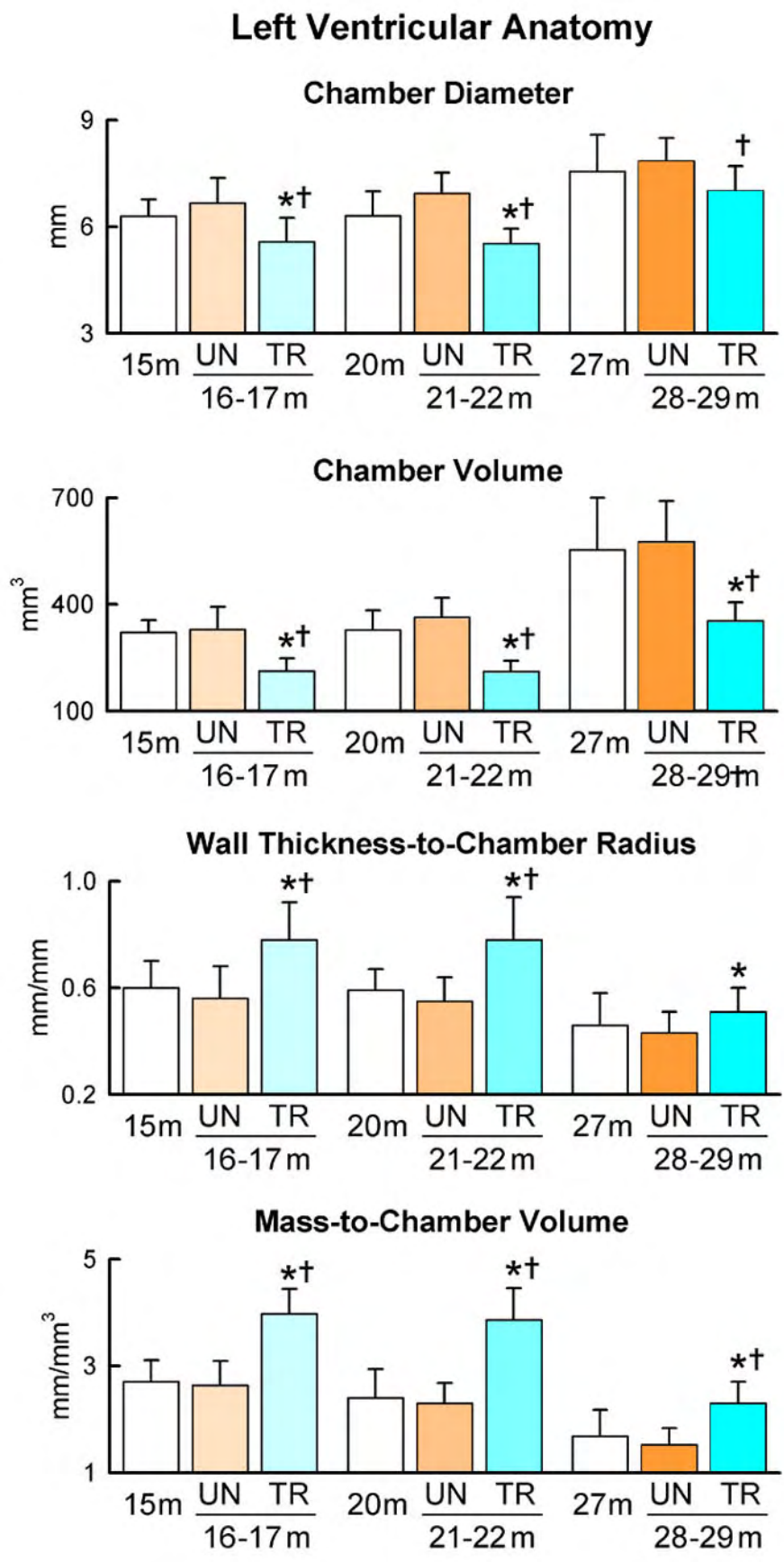
Left Ventricular Anatomy
Chamber Diameter
mm
9
6
3
*†
*†
†
15m UN TR 20m UN TR 27m UN TR
16-17 m
21-22 m
28-29 m
Chamber Volume
mm3
700
400
100
*†
*†
*†
15m UN TR 20m UN TR 27m UN TR
16-17 m
21-22 m
28-29 m
Wall Thickness-to-Chamber Radius
mm/mm
1.0
0.6
0.2
*†
*†
*
15m UN TR 20m UN TR 27m UN TR
16-17 m
21-22 m
28-29 m
Mass-to-Chamber Volume
mm/mm3
5
3
1
*†
*†
*†
15m UN TR 20m UN TR 27m UN TR
16-17 m
21-22 m
28-29 m

Figure XVI

Untreated

baseline

45 days

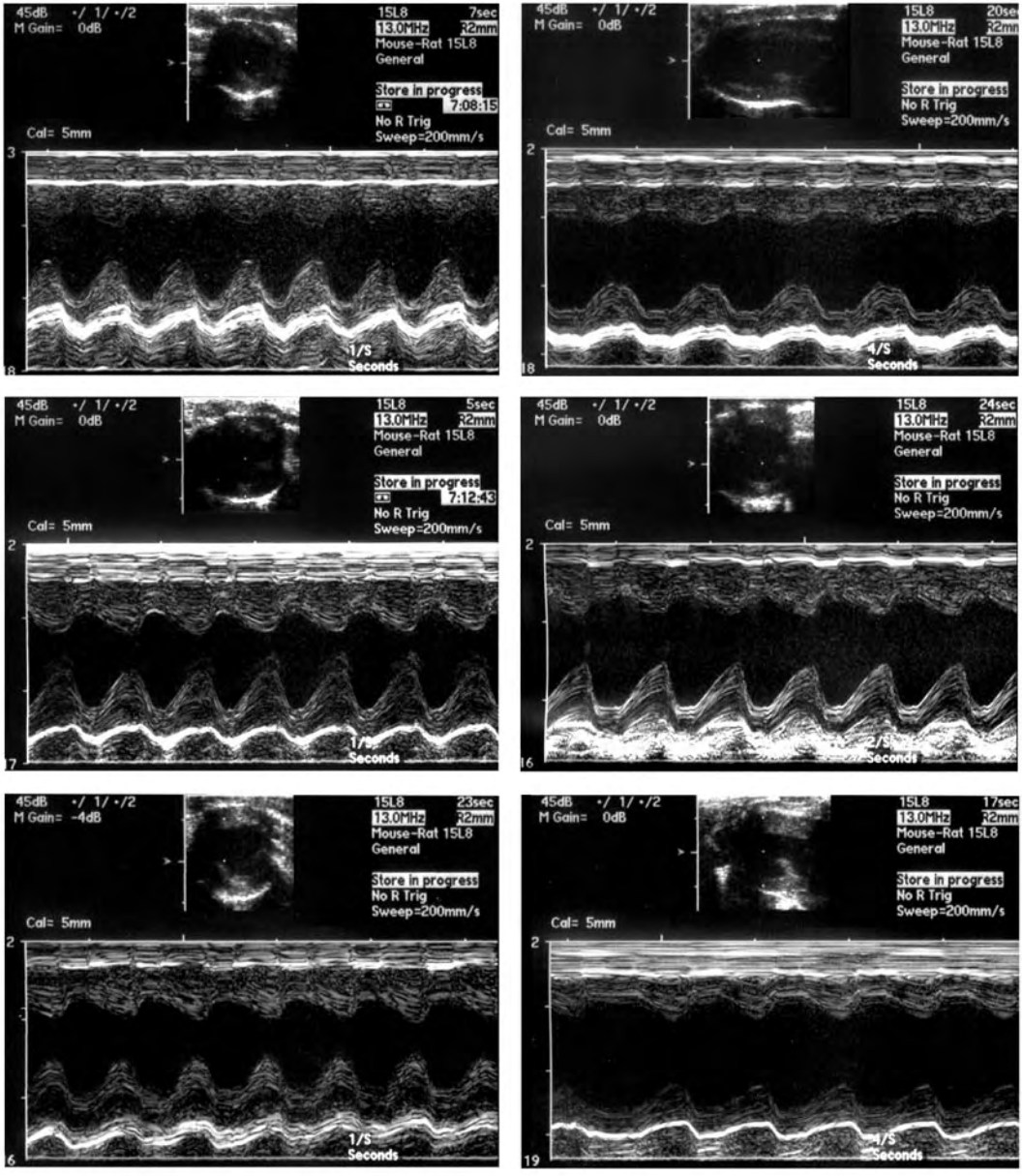

A

Figure XVII A

Treated

baseline

45 days

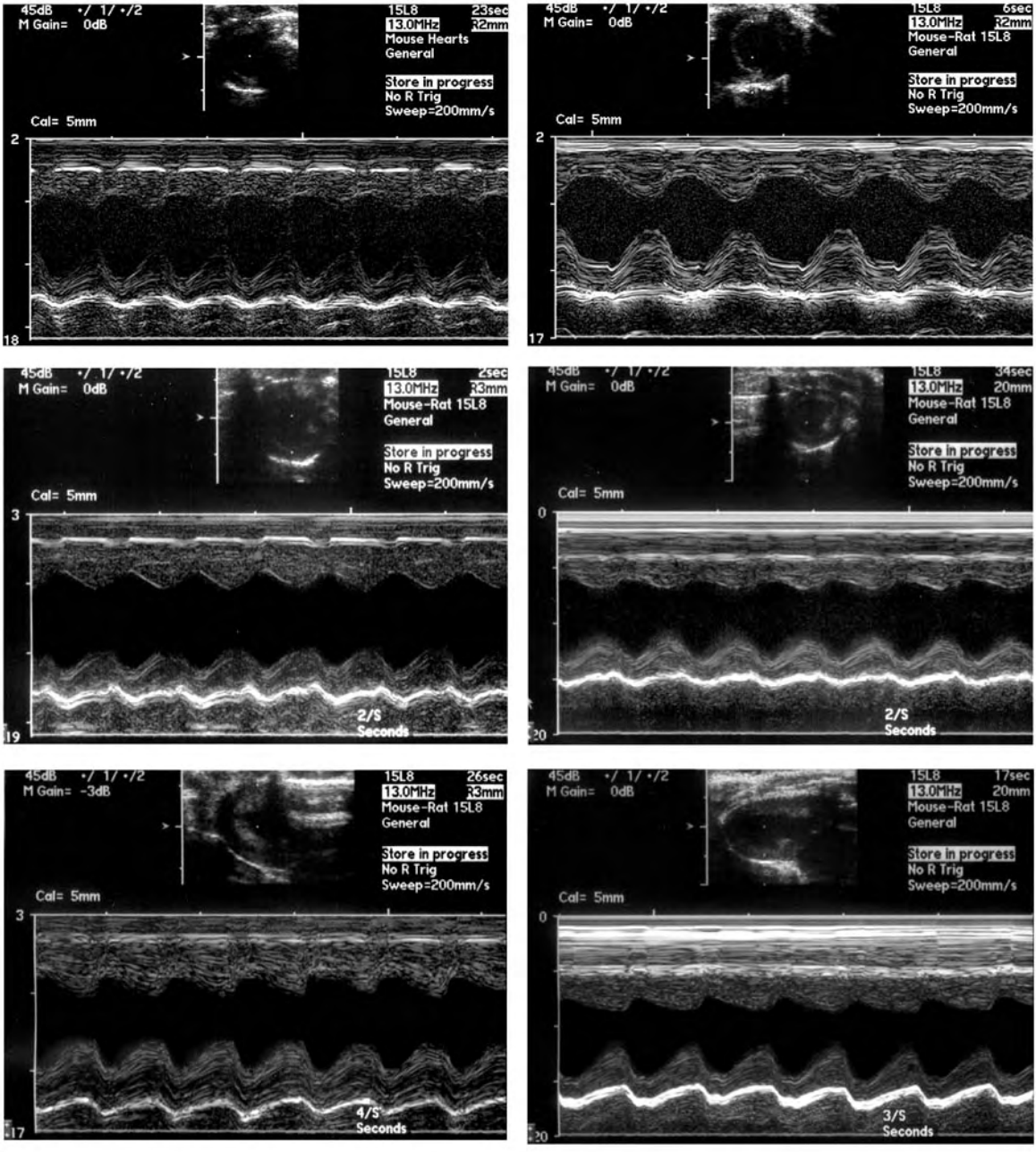

B

Figure XVII B